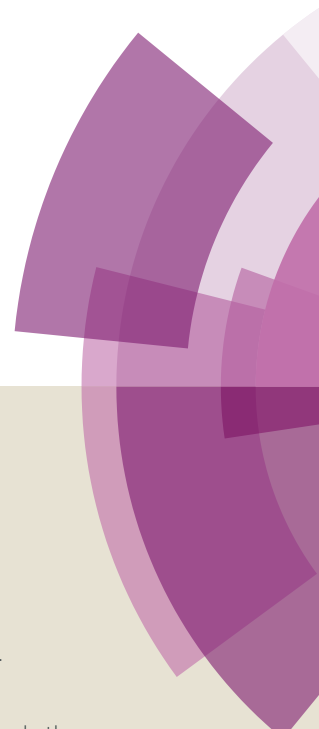


Dalton Transactions

Accepted Manuscript



This article can be cited before page numbers have been issued, to do this please use: L. Rigamonti, A. Forni, S. Righetto and A. Pasini, *Dalton Trans.*, 2019, DOI: 10.1039/C9DT01216H.



This is an Accepted Manuscript, which has been through the Royal Society of Chemistry peer review process and has been accepted for publication.

Accepted Manuscripts are published online shortly after acceptance, before technical editing, formatting and proof reading. Using this free service, authors can make their results available to the community, in citable form, before we publish the edited article. We will replace this Accepted Manuscript with the edited and formatted Advance Article as soon as it is available.

You can find more information about Accepted Manuscripts in the [author guidelines](#).

Please note that technical editing may introduce minor changes to the text and/or graphics, which may alter content. The journal's standard [Terms & Conditions](#) and the ethical guidelines, outlined in our [author and reviewer resource centre](#), still apply. In no event shall the Royal Society of Chemistry be held responsible for any errors or omissions in this Accepted Manuscript or any consequences arising from the use of any information it contains.

Push-pull unsymmetrical substitution in nickel(II) complexes with tetradentate N_2O_2 Schiff base ligands: synthesis, structures and linear-nonlinear optical studies†

Luca Rigamonti,^{*a,c} Alessandra Forni,^{*b,c} Stefania Righetto^c and Alessandro Pasini^c

^a Dipartimento di Scienze Chimiche e Geologiche, Università degli Studi di Modena e Reggio Emilia, via G. Campi 103, 41125 Modena, Italy

Email: luca.rigamonti@unimore.it, luca.rigamonti@yahoo.com

^b Istituto di Scienze e Tecnologie Molecolari, Consiglio Nazionale delle Ricerche (ISTM-CNR), via Golgi 19, 20133 Milano, Italy

Email: a.forni@istm.cnr.it

^c Dipartimento di Chimica, Università degli Studi di Milano, via C. Golgi 19, 20133 Milano, Italy

† Electronic supplementary information (ESI) available. CCDC 1903483–1903485 for **3c**·CHCl₃, **3g**·EtOH and **3j**, respectively; Experimental Section (cont.); Crystallographic and data collection parameters for **3c**·CHCl₃, **3g**·EtOH and **3j** (Table S1); Computed excitation energies, oscillator strengths and analysis of the most important contributions to the transitions for compounds **3** and selected analogue copper(II) complexes (Table S2); Isodensity surface plot of the PBE0/6-311++G(d,p) frontier orbitals of **3c** and **3j** mainly involved in the computed transitions (Fig. S1); UV-visible absorption spectra of **3c**: dilution studies from 10⁻³ down to 10⁻⁵ mol L⁻¹ CHCl₃ solutions, solvatochromism at 5 × 10⁻⁵ mol L⁻¹ solutions in solvents from low polar toluene to high polar methanol, and addition of increasing amount of DMSO to the 10⁻⁴ mol L⁻¹ CHCl₃ solution (Fig. S2); UV-visible absorption spectra of **3j**: solvatochromism at 5 × 10⁻⁵ mol L⁻¹ solutions in solvents from low polar toluene to high polar methanol, and addition of increasing amount of DMSO to the 10⁻⁴ mol L⁻¹ CHCl₃ solution (Fig. S3). For ESI and crystallographic data in CIF or other electronic format see DOI: 10.1039/***.

Abstract

New push-pull (A–D) nickel(II) compounds of general formula [Ni(5-A-5'-D-saltn)] (**3a–3l**) with unsymmetrically-substituted N_2O_2 tetradentate Schiff base ligands are here reported. The ligands 5-A-5'-D-saltn²⁻ (H₂saltn = *N,N'*-bis(salicylidene)diaminopropane) possess differently-substituted salicylaldehyde (^{A/D}sal) moieties condensed to 1,3-diaminopropane (tn), carrying either an electron acceptor (A = H, Br, NO₂) or donor (D = H, Me, OMe) group in *para* position with respect to the coordinated phenoxido oxygen atoms. These compounds could be obtained by template synthesis involving derivatives [Ni(^Gsal)₂(H₂O)₂], **1a–e** (G = NO₂, Br, H, Me and OMe, respectively) and [Ni(^GL)₂], **2a–d** (^GL⁻ = (*E*)-2-((3-aminopropylimino)methyl)-4-G-phenolate, G = NO₂, Br, H

and Me, respectively). Refluxing compounds **1** and **2** carrying G groups suitable for the desired final A–D combination, scrambling of the ligands occurred and condensation to compounds **3** was suitably achieved. Dinuclear intermediates $[\text{Ni}_2(\mu\text{-}^G\text{L})_2(\text{G}^i\text{sal})_2]$ (**4a,b,e,f,g**) were also detected and isolated. The single-crystal X-ray diffraction structures of $[\text{Ni}(5'\text{-OMe-saltn})\cdot\text{CHCl}_3]$ (**3c**·CHCl₃), $[\text{Ni}(5\text{-Br-5}'\text{-OMe-saltn})\cdot\text{EtOH}]$ (**3g**·EtOH) and $[\text{Ni}(5\text{-NO}_2\text{-saltn})]$ (**3j**) show different degrees of distortion around the central core, leading to saddle-like (**3c**), planar (**3g**) and step-like (**3j**) molecular conformations. DFT geometry optimization of compounds **3** shows that, for isolated molecules, the saddle-like conformation is slightly more stable with respect to the other ones. UV-visible absorption spectra show structured absorption profiles at about 320–440 nm, whose intensity is amplified by the presence of the nitro group, assigned to a convolution of one metal-to-ligand charge transfer and two intra-ligand charge transfer transitions by TDDFT computations. Surprisingly, UV-visible spectra of derivatives with Br are comparable with the ones with Me, suggesting in this case a behaviour of the halogen as a weak electron donor group. The experimental investigation (through Electric-Field-Induced Second-Harmonic and solvatochromic measurements) of the second-order NLO responses of compounds **3**, in conjunction with theoretical calculations, reveals that the observed NLO efficiency is determined by the combined effect of two almost orthogonal charge transfer directions within the molecules, one along the axis approximately bisecting the donor and the accepting moieties and the other along the A–D axis.

Introduction

Nonlinear optics (NLO)^{1–8} started to be explored by Franken et al in 1961 with the discovery of second-harmonic generation (SHG), or frequency doubling,⁹ right after the construction of the first laser by Maiman in 1960.^{10,11} In fact, only when the time-varying electric component **E** of the electromagnetic light wave, and at intensities as observed in a laser light beam, is applied, a molecule (material) can respond nonlinearly to **E**, and the microscopic (macroscopic) polarization **p** (**P**) can be expressed by the power series in the field strength: $\mathbf{p} = \alpha \mathbf{E} + \beta \mathbf{E}\cdot\mathbf{E} + \gamma \mathbf{E}\cdot\mathbf{E}\cdot\mathbf{E} + \dots$ ($\mathbf{P} = \chi^{(1)} \mathbf{E} + \chi^{(2)} \mathbf{E}\cdot\mathbf{E} + \chi^{(3)} \mathbf{E}\cdot\mathbf{E}\cdot\mathbf{E} + \dots$), where α is the linear polarizability and β and γ are the quadratic and cubic hyperpolarizabilities, respectively ($\chi^{(i)}$ are the electric susceptibility coefficients of *i* order),⁵ and the β tensor (or $\chi^{(2)}$) is the responsible for the second-order NLO response.¹² Since the discovery, NLO has then started finding different applications with growing impact on today's daily life.¹³

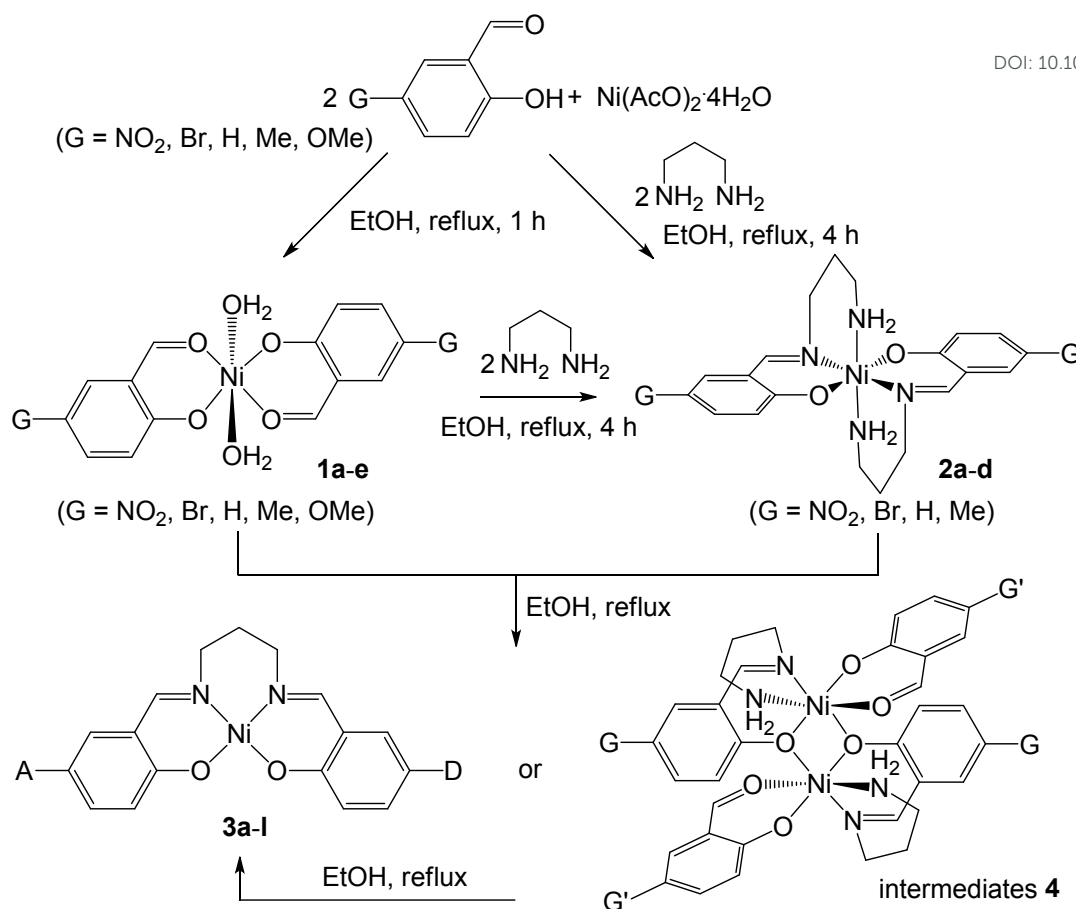
The interest in this field, and in particular in the second-order behaviour,¹⁴ has led to the synthesis of several compounds during years bearing a dipolar acceptor- π -bridge-donor (A- π -D)

molecular architecture,^{15–18} which gives rise to a non-zero β value due to polarizable electrons in a non-centrosymmetric environment. Organic derivatives have shown to possess large and very fast quadratic NLO responses^{16,18} that can be enhanced by increasing donor or acceptor strength,^{19,20} or by molecular skeleton modifications.^{17,21–23} Organometallic and coordination compounds have been also actively investigated for NLO applications since they offer a larger variety of molecular structures compared to pure organic systems.^{24–34} In particular, the electronic properties are modulated by the *d*- and *f*-electrons²⁶ of the metal ions,³⁵ since the metal-containing moiety of the molecule can act as either donor^{30,36,37} or acceptor group,^{38,39} and the existence of different oxidation states for the same metal can act as a switch of the NLO properties by redox reactions.^{40–44} Supramolecular assemblies of coordination units into metal-organic frameworks have also shown to be competitive materials for NLO applications.^{8,45,46}

Metal complexes with tetradentate N₂O₂ salen-type Schiff bases are particularly interesting for their NLO features^{25,27,29,47,48} because of the high thermal and chemical stability⁴⁹ and the non-innocent role of the metal centre as bridge between the acceptor A and the donor D groups, positioned on the organic skeleton of the compounds, and this is due to the presence of charge transfer (CT) transitions at low energies that involve the metal ion.^{38,50–62} Moreover, they show the possibility to be incorporated into polymers and create NLO-active thin films.^{63,64} The second-order NLO properties of these compounds have been studied in complexes with D groups (OMe, NEt₂) in position 4 of the salicylaldehyde (sal) moieties and A groups (NO₂, Cl) on the *o*-phenyldiamine (*o*-phen), where this substitution increases the charge asymmetry of the final [M(salophen)] (M = Co, Ni, Cu, Zn) structure and enhances their NLO responses.^{54,55,57} As a matter of fact, nickel(II) is among the most studied transition metals in this class of compounds^{49,50,53–55,57–59,61,62,65} thanks to its role in the NLO efficiency and its inclination for the square planar coordination environment.⁶⁶

With the scope of increasing the knowledge on salen-type complexes, few years ago we started studying salen analogues where the two sal moieties bear different substituents in position 5, i.e. *para* to the coordinated phenoxido oxygen atom. Our first results regarded the copper(II) complexes of general formula [Cu(5-A-5'-D-salen)] and [Cu(5-A-5'-D-saltn)],³⁸ in which the acceptor group was mainly NO₂ while the D groups were H, Me, OMe and NMe₂ (tn = 1,3-diaminopropane). In these compounds, the induced charge asymmetry generated by the A–D unsymmetrical substitution leads to the concomitant modulation of the μ_g (ground state electric dipole moment) and β_{tot} (derived from the full β hyperpolarizability tensor) vector directions. More recently, unsymmetrically substituted zinc(II) and nickel(II) salophen complexes were also reported and studied for their third-order (two-photon absorption) NLO properties.⁶⁷

The present work aims to a further step in the electronic features and linear and second-order NLO behaviours of salen-type derivatives with the flexible aliphatic diamine **tn**, studying the effect of the metal change from copper(II) to nickel(II) in the molecular core of **saltn** ligands. In fact, the modulating role of the metal centre in the NLO response of these class of complexes with tetradentate Schiff base ligands^{51,53} is worthy to be investigated, in addition to the possibility for the coordination geometry to move away from a strictly square planar geometry (as for **salophen** ligands) thanks to the propylene bridge, which allows the access to more low-lying excited states other than the only metal-centred charge transfer transition with concomitant enhancement of the NLO responses.^{53,68} The template synthesis⁶⁹ of the compounds [Ni(5-A-5'-D-**saltn**)] (**3a-l**, see Table 1 and Scheme 1 for A–D substitutions) is here exploited by reaction of derivatives [Ni(^Gsal)₂(H₂O)₂], **1a-e** (G = NO₂, Br, H, Me and OMe, respectively) with [Ni(^GL)₂], **2a-d** (^GL⁻ = (*E*)-2-((3-aminopropylimino) methyl)-4-G-phenolate, G = NO₂, Br, H and Me, respectively). The isolation of some reaction intermediates **4** with probable dinuclear structure⁷⁰ and peculiar reactivity depending on the substituents will be also presented (see Scheme 1). The experimental and theoretical characterizations of the linear and nonlinear optical features and the comparison with the analogue copper(II) compounds³⁸ will be then described, in order to clarify the role of the metal, and with the extension in the use of bromine as further electron-active substituent.



Scheme 1 Synthetic scheme with reaction conditions of all synthetic steps from precursors **1** and **2** to intermediates **4** and final products **3**.

Table 1 Combinations in the reaction between derivatives **1** and **2** and final A–D complexes **3**, together with the isolated intermediates **4** (see Scheme 1).

reaction	compound	A	D	yield %	intermediate	G	G'	yield %
–	3a	H	H	73	4a	H	H	35
1d + 2c	3b	H	Me	–	4b	H	Me	42
1c + 2d					4b'	Me	H	47
1e + 2c	3c	H	OMe	68	not detected			
–	3d	Br	Br	70	–			
1c + 2b	3e	Br	H	–	4e	Br	H	80
1b + 2c					4e'	H	Br	49
1d + 2b	3f	Br	Me	67	4f	Br	Me	75
1b + 2d					not detected			
1e + 2b	3g	Br	OMe	37	4g	Br	OMe	67
–	3h	NO ₂	NO ₂	80	–			
1a + 2b	3i	NO ₂	Br	82	not detected			
1b + 2a					not detected			

1c + 2a	3j	NO ₂	H	66	not detected	View Article Online DOI: 10.1039/C9DT01216H
1a + 2c				55	not detected	
1d + 2a	3k	NO ₂	Me	50	not detected	
1a + 2d				85	not detected	
1e + 2a	3l	NO ₂	OMe	–	not detected	

Experimental section

General information

All used chemicals were reagent grade. Solvents were used as received. Elemental analyses were performed at the Microanalytical Laboratory at the Università degli Studi di Milano. ESI-MS spectra were recorded in MeOH solutions with a LCQ Advantage Thermofluxional instrument. Infrared spectra were recorded as KBr disks using a JASCO FT-IR 410 spectrophotometer with a 2 cm⁻¹ resolution. UV-visible spectra for all soluble compounds **1**, **2** and **3** of 10⁻⁴ mol L⁻¹ CHCl₃ solution at 298 K were recorded with a Hewlett Packard 8453 spectrophotometer; dilution studies for **3c** and **3j** from 10⁻³ down to 5 × 10⁻⁶ mol L⁻¹ CHCl₃ solutions at 298 K were performed with a Jasco V-570 UV/Vis/NIR spectrophotometer, which was also employed for solvatochromism studies of **3c** and **3j** at 5 × 10⁻⁵ mol L⁻¹ solutions in the following solvents (Reichardt polarity parameters $E_T(30)^{71,72}$ in kcal mol⁻¹ and relative polarity to water⁷³ are reported in brackets): toluene (33.9, 0.099), THF (37.4, 0.207), AcOEt (38.1, 0.228), CHCl₃ (39.1, 0.259), CH₂Cl₂ (41.1, 0.309), acetone (42.2, 0.355), DMF (43.8, 0.386), DMSO (45.0, 0.444), CH₃CN (46.0, 0.460), EtOH (51.9, 0.654) and MeOH (55.5, 0.762); λ values are accurate to ± 1 nm and spectra are mainly reported as wavenumbers, cm⁻¹ (ϵ , L mol⁻¹ cm⁻¹). ¹H NMR spectra were recorded on a 400 MHz Bruker FT-NMR Advance400 spectrometer at 298 K in CDCl₃ as solvent; chemical shifts are given in parts per million (ppm) versus external TMS and were determined by reference to the solvent residual signals (7.26 ppm for CHCl₃).

Synthetic procedures for compounds **1**

[Ni(^{NO₂sal})₂(H₂O)₂] (**1a**).^{74–76} 5-NO₂-salH (517.0 mg, 3.10 mmol) was dissolved in ethanolic KOH (6.2 mL of a 0.5 mol L⁻¹ solution, 3.10 mmol) and solid Ni(AcO)₂·4H₂O (384.5 mg, 1.55 mmol) was added under stirring. The mixture was refluxed for 1 h and then cooled down, yielding the product as green solid, filtered, washed with EtOH and diisopropyl ether (iPr₂O) and dried under vacuum (597.9 mg, 98%). Anal. Calcd (%) for C₁₄H₁₂N₂NiO₁₀ (426.95): C, 39.38; H, 2.83; N, 6.56. Found: C, 39.08; H, 3.00; N, 6.34. IR (KBr): 3437 (ν_{O-H}), 1633 ($\nu_{C=O}$), 1306 (ν_{NO_2}) cm⁻¹. UV-vis: not soluble in CHCl₃. Syntheses of **1b–1e** and their characterization can be found in the Electronic Supplementary Information (ESI).

Synthetic procedures for compounds 2

[Ni(^{NO₂L})₂] (2a). 5-NO₂-salH (840.0 mg, 5.03 mmol) was dissolved in ethanolic KOH (50.0 mL of a 0.1 mol L⁻¹ solution, 5.00 mmol), and Ni(AcO)₂·4H₂O (624.5 mg, 2.51 mmol) was added under stirring. The light yellow mixture was heated at 70 °C for 1 h, then tn (630 μL, 7.55 mmol) was added and the mixture was refluxed for 3 h. After cooling, **2a** was recovered by filtration as yellow solid, washed with EtOH, acetone and dried under vacuum (1214.1 mg, 96%). Anal. Calcd for C₂₀H₂₄N₆NiO₆ (503.14): C, 47.74; H, 4.81; N, 16.70. Found: C, 47.81; H, 4.90; N, 16.61. MS (ESI): *m/z* 525 ([M + Na]⁺, 80%), 1027 ([2M + Na]⁺, 100). IR (KBr): 3313, 3257 (ν_{NH₂}), 1640, 1595 (ν_{C=N}), 1312, 1289 (ν_{NO₂}) cm⁻¹. UV-vis (CHCl₃): 25710 (12550). Syntheses of **2b–2d** and their characterization can be found in the ESI.

Synthetic procedures for compounds 3 and 4

[Ni(saltn)] (3a). *First method:* This compound was synthesized with a modification of literature procedures.^{77,78} salH (116.8 mg, 0.96 mmol) and tn (40 μL, 0.48 mmol) were dissolved in EtOH (15 mL) and the yellow mixture was refluxed for 30 minutes. NiCl₂·6H₂O (116.8 mg, 0.49 mmol) and Et₃N (1 mL) were then added and the brownish mixture was refluxed for 4 h. After one night at room temperature, the compound precipitated as green crystals, filtered, washed with EtOH, ⁱPr₂O and dried under vacuum (127.5 mg, 73%). Anal. Calcd (%) for C₁₇H₁₆N₂NiO₂·1.5H₂O (366.04): C, 55.78; H, 5.23; N, 7.65. Found: C, 55.37; H, 5.22; N, 7.71. MS (ESI): *m/z* 339 ([M + 1]⁺, 100%). IR (KBr): 3454 (ν_{O-H}), 1621 (ν_{C=N}) cm⁻¹. *Second method:*⁷⁹ **isolation of the intermediate [Ni₂(μ-HL)₂(^Hsal)₂] (4a).** tn (61 μL, 0.73 mmol) was added to a suspension of **1c** (245.2 mg, 0.73 mmol) in EtOH (15 mL) and the mixture was heated to reflux, which causes the complete dissolution and the formation of a green solution. After few minutes a green crystalline solid precipitated and the mixture was further refluxed for 2 h. After cooling, the intermediate **4a** was filtered, washed with EtOH, ⁱPr₂O and dried under vacuum (89.8 mg, 35%). Anal. Calcd (%) for C₃₄H₃₆N₄Ni₂O₆ (714.06): C, 57.19; H, 5.08; N, 7.85. Found: C, 56.75; H, 5.31; N, 7.65. IR (KBr): 3344, 3290 (ν_{NH₂}), 1633 (ν_{C=N}) cm⁻¹. The green compound **4a** (85.0 mg, 0.13 mmol) was suspended again in EtOH (50 mL) and refluxed for other 2 h, till the solid completely dissolved. The brown solution obtained was left standing at room temperature for two days till brown needles of **3a** precipitated that were filtered, washed with EtOH and dried under vacuum (53.2 mg, 66%). Anal. Calcd (%) for C₁₇H₁₆N₂NiO₂ (339.03): C, 60.23; H, 4.76; N, 8.26. Found: C, 60.71; H, 5.04; N, 7.72. IR (KBr): 1621 (ν_{C=N}) cm⁻¹.

[Ni(5'-Me-saltn)] (3b) and isolation of the intermediates [Ni₂(μ-HL)₂(Me^Hsal)₂] (4b) and [Ni₂(μ-Me^LL)₂(H^{sal})₂] (4b'). *First method 1d + 2c*: **1d** (123.9 mg, 0.30 mmol) and **2c** (109.5 mg, 0.30 mmol) were suspended in EtOH (30 mL) and left under reflux for 5 h. The intermediate **4b** was filtered as light green solid, washed with EtOH, ⁱPr₂O and dried in vacuo (107.9 mg, 42%). Anal. Calcd (%) for C₃₆H₄₀N₄Ni₂O₆·EtOH·4H₂O (860.24): C, 53.06; H, 6.33; N, 6.51. Found: C, 53.09; H, 6.33; N, 6.45. MS (ESI): *m/z* 235 ([Ni(HL)]⁺, 40%), 253 ([Ni(HL)(H₂O)]⁺, 100). IR (KBr): 3452 (ν_{O-H}), 3348, 3288 (ν_{NH2}), 1633 (ν_{C=N}). Further refluxing in EtOH or drying under vacuum of **4b** did not yield **3b**. *Second method 1c + 2d*: **1c** (111.5 mg, 0.33 mmol) was dissolved in EtOH (20 mL) and **2d** (157.5 mg, 0.31 mmol) was added, yielding a green suspension that was refluxed for 5 h. The intermediate **4b'** was recovered by filtration as light green solid, washed with ⁱPr₂O and dried under vacuum (107.7 mg, 47%). Anal. Calcd (%) for C₃₆H₄₀N₄Ni₂O₆ (742.11): C, 58.26; H, 5.43; N, 7.55. Found: C, 58.50; H, 5.74; N, 7.39. MS (ESI): *m/z* 249 ([Ni(Me^LL)]⁺, 25%), 267 ([Ni(Me^LL)(H₂O)]⁺, 100). IR (KBr): 3346, 3287 (ν_{NH2}), 1648 sh, 1634 (ν_{C=N}) cm⁻¹. **4b'** and the left reaction mixture were further mixed together and refluxed for other 5 h, obtaining **3b** as light green solid, which was filtered, washed with ⁱPr₂O and dried under vacuum (85.1 mg, 39%). Anal. Calcd (%) for C₁₈H₁₈N₂NiO₂·H₂O (371.06): C, 58.26; H, 5.43; N, 7.55. Found: C, 58.28; H, 5.51; N, 7.59. MS (ESI): *m/z* 353 ([M + 1]⁺, 100%), 707 ([2M + 1]⁺, 60), 727 ([2M + Na]⁺, 70). IR (KBr): 3438 (ν_{O-H}), 1627 (ν_{C=N}) cm⁻¹. ¹H NMR (CDCl₃, 298 K, 400 MHz): δ 1.32 (2H, H₂O), 1.90 (2H, tn central CH₂), 2.23 (3H, Me), 3.56 (4H, tn lateral CH₂), 6.5–7.1 (9H, aromatic and N=CH) ppm. Syntheses of all other derivatives **3** and **4** and their characterization can be found in the ESI.

X-ray crystal structure determinations

Single crystals suitable for X-ray diffraction of **3c** (H,OMe) and **3j** (NO₂,H) were obtained from slow diffusion of ⁱPr₂O into CHCl₃ solutions, while for **3g** (Br,OMe) were obtained from slow diffusion of *n*-hexane into an EtOH solution. Crystal data and details of data collection and refinement are given in Table S1 in the ESI. Intensity data for all compounds were collected on a Bruker Apex CCD area detector using graphite monochromatic Mo-*K*α radiation. During data collections, no crystal decay was observed, so that no time-decay correction was needed. Data reductions were performed with SAINT, and absorption corrections based on multiscan were obtained with SADABS.⁸⁰ All the structures were solved by direct methods and refined with SHELXL-2014/7⁸¹ implemented in WinGX–2014.1 system.⁸² The program ORTEPIII was used for graphics.⁸³ Anisotropic thermal parameters were used for all non-hydrogen atoms. The isotropic thermal parameters of H atoms were fixed at 1.2 (1.5 for methyl groups) times those of the atom to which they were attached. All H atoms were placed in calculated positions and refined by a riding model. Complete crystallographic data were deposited at the Cambridge Crystallographic Data

Centre (CCDC 1903483–1903485 for **3c**·CHCl₃, **3g**·EtOH and **3j**, respectively). These data can be obtained free of charge from the CCDC via www.ccdc.cam.ac.uk/data_request/cif. View Article Online
DOI: 10.1039/C9DT01216H

Second-order NLO measurements

EFISH measurements of derivatives **3**, with the exception of **3d** (Br,Br) and **3h** (NO₂,NO₂) due to their too low solubility, were carried out in CHCl₃ solutions (concentrations ranging from 5×10^{-4} to 7×10^{-5} mol L⁻¹) working at non-resonant incident wavelength $\lambda = 1.907 \mu\text{m}$, using a Q-switched, mode-locked Nd³⁺:YAG laser (Atalaser), equipped with a Raman shifter; the apparatus for the EFISH measurements was made by SOPRA (France). The NLO molecular responses were measured by the solution-phase direct current EFISH generation method. It provides γ_{EFISH} , the direct information on the molecular NLO properties, through the following equation:

$$\gamma_{\text{EFISH}} = (\mu_{\text{g}}\beta_{\text{vec}} / 5kT) + \chi(-2\omega, \omega, \omega, 0) \quad (1)$$

where $\mu_{\text{g}}\beta_{\text{vec}}/5kT$ is the dipolar orientational contribution, with $\beta_{\text{vec}} = (5/3)\beta_{\parallel}$ (see note of Table 8) being the projection along the dipole moment axis of the vectorial component of the quadratic hyperpolarizability tensor β , and $\chi(-2\omega, \omega, \omega, 0)$ is the cubic electronic contribution to γ_{EFISH} , which can be considered negligible for the kind of push-pull molecules here investigated. Such hypothesis was verified by performing $\gamma_{\text{THG}}(-3\omega, \omega, \omega, \omega)$ measurements for **3c** and **3j** derivatives in 2×10^{-4} mol L⁻¹ CHCl₃ solutions, using the same SOPRA instrument, and comparing the ‘purely’ cubic contribution to hyperpolarizability, γ_{THG} , with the ‘mixed’ quadratic/cubic one, γ_{EFISH} . Since the measured γ_{THG} , 0.07 and 0.02×10^{-33} esu for **3c** and **3j** respectively, were lower than the 5% of γ_{EFISH} , falling in the $3\text{--}6 \times 10^{-33}$ esu for all derivatives, the third order contribution of Eq. (1) can be confidently considered as negligible.

Computational details

Benchmark DFT and TDDFT calculations were performed on **3c** (H,OMe) in order to fix the protocol to be used for all compounds **3**. The X-ray molecular structure of **3c** (H,OMe), rather than that of **3g** (Br,OMe) or **3j** (NO₂,H), was in fact deemed the most appropriate one to be used as starting point for geometry optimization of all complexes, after substitution of OMe with the proper D group and of H on the opposite side with the desired A group. On one side, in fact, the presence of strongly interacting dimers in **3g** (see below, Crystal structures description) was presumably responsible for an otherwise unexpected almost planar conformation of the complex. To verify such hypothesis, we performed a geometry optimization of a head-to-tail dimer of **3c**, starting from the corresponding experimental one where molecules are laterally shifted giving rise to weak intradimer interaction. In the optimized **3c** dimer, molecules are almost overlapped and

significantly more planar with respect to the ‘saddled-shaped’ geometry as obtained for the isolated molecule, which is close to the experimental one, confirming that strong π - π interactions in solid state, as observed in **3g**, induce a greater planarity with respect to that expected in solution. On the other side, the molecular structure of **3j** is characterized by a quite distorted ‘step-like’ conformation, which was not deemed to be representative for the whole series of complexes. We individuated the origin of such distortion in the conformation of the tn (C1–C2–C3) bridge. In the case of **3c**, C1 and C2 are placed on the same side with respect to the N₂O₂ coordination plane, with C3 lying on this plane, while in **3j** C1 and C3 are on either sides with respect to the N₂O₂ plane, which contains also C2. Geometry optimization of **3c** starting from the latter conformation led in fact to a ‘step-like’ structure, quite similar to that of **3j**, which was 0.29 kcal mol⁻¹ less stable than the saddle-shaped one. Therefore, the form with tn bridge on the same side with respect to the N₂O₂ plane was deemed statistically more probable in solution than the other one, though its presence should not be excluded. It is to be noted that this conformation corresponds to the ‘up’ isomer as defined in our previous theoretical analysis of [Cu(5-A-5'-D-saltn)] complexes.³⁸

To assess the most appropriate protocol for DFT and TDDFT calculations, we first evaluated the better performance between the B3LYP^{84–86} and the M06⁸⁷ functionals in reproducing the experimental geometry of **3c**, using the 6-311++G(d,p) basis set. The former functional was used owing to its widely recognized performance, while the latter was tested because it was properly developed to treat organometallic complexes. On average, a slightly better agreement with the experimental structure was obtained with the M06 functional, which was then adopted for all geometry optimizations. Two functionals were then tested to compute the excitation energies, i.e. M06-2X⁸⁷ and PBE0,^{88,89} both of them having been suggested for simulations of absorption spectra of organic and organometallic molecular compounds.^{90–93} While both functionals well reproduced the overall features of the observed UV-vis spectrum of **3c**, the M06-2X excitation energies were significantly shifted towards high energies while a good numerical agreement was obtained using PBE0, which was then adopted for TDDFT calculations. SHG hyperpolarizabilities, i.e. the $\beta(-2\omega, \omega, \omega)$ tensors, were computed within the Coupled Perturbed Kohn–Sham (CPKS) approach at the same frequency as used as in the EFISH experiments. To further confirm the hypothesis of negligible third order contribution coming from the EFISH measurements (Eq. 1), additional calculations were performed on **3c** and **3j** to evaluate, by Finite Field technique, the SHG second hyperpolarizabilities, i.e. the $\chi(-2\omega, \omega, \omega, 0)$ tensors. The resulting γ_{\parallel} was 15.6 and 8.4% with respect to $\mu_g \beta_{\text{vec}} / 5kT$ ($T = 298$ K) for **3c** and **3j**, respectively, confirming the predominant contribution of the second-order term in the EFISH measurements for this class of compounds. The CAM-B3LYP functional,⁹⁴ which has been recently recommended for hyperpolarizability calculations of mid-size organic chromophores,⁹⁰ was adopted. A pruned (99,590) grid was selected for computation and

use of two-electron integrals and their derivatives. The solvent (CHCl_3) effect on the computed β 's was taken into account through the PCM approach based on the integral equation formalism model (IEFPCM).⁹⁵ All calculations were performed with the Gaussian16 suite of programs.⁹⁶

View Article Online
DOI: 10.1039/C9DT01216H

Results and discussion

Template synthesis and spectroscopic characterization

Reaction of $\text{Ni}(\text{AcO})_2 \cdot 4\text{H}_2\text{O}$ with two moles of substituted 5-G-salH yields the compounds **1a–e** of general formula $[\text{Ni}(\text{Gsal})_2(\text{H}_2\text{O})_2]$ ($\text{G} = \text{NO}_2$,^{74–76} Br ,^{74,75} H ,^{74,75,97,98} Me , OMe , respectively) in which the nickel(II) ion brings two coordinated deprotonated salicylaldehydato anions occupying the square planar plane and two apical water molecules.^{74–76,97–99} Subsequent addition of ≈ 2.5 moles (excess) of tn to derivatives **1**, or direct synthesis without isolation of **1** starting from 5-G-salH: $\text{Ni}(\text{AcO})_2 \cdot 4\text{H}_2\text{O}$:tn in a 2:1:2.5 ratio, led to obtain compounds **2a–d** of general formula $[\text{Ni}(\text{GL})_2]$ ($\text{G} = \text{NO}_2$, Br ,^{100,101} H ,¹⁰² Me , respectively) in excellent yields. The hypothetical product **2e** starting from 5-OMe-salH could not be isolated, maybe due to the high solubility given by the methoxy group; any attempt of precipitation or isolation led to decomposition to undesired products. In compounds **2** the nickel(II) ion is hexa-coordinated in an octahedral fashion, with two tridentate NNO Schiff base ligands GL^- , obtained from the mono-condensation of one mole of 5-G-salH with tn. There are some examples of the synthesis^{100,102–104} and crystal structures^{101,105–108} of these kind of compounds in the literature, as well as similar complexes with different carbonyl derivatives^{109,110} or diamines.^{111–113} By the way, this synthetic methodology cannot be applied using 1,2-ethanediamine (en), since it leads to the symmetric bicondensed product $[\text{Ni}(\text{salen})]$, probably due to the strained 5-membered metallacycle. Main infrared peaks and UV-visible absorption bands of compounds **1** and **2** are reported in Table 2.

The synthesis of the unsymmetrically-substituted $[\text{Ni}(5\text{-A-5}'\text{-D-saltn})]$ compounds, **3b**, **3c**, **3e**, **3f**, **3g**, **3i**, **3j**, **3k** and **3l** ($\text{A} = \text{H}$, Br , NO_2 ; $\text{D} = \text{H}$, Me , OMe , or Br only with the nitro group as A), was achieved using the template path reported in Scheme 1 from the reaction under reflux in ethanol of the appropriate derivatives **1** and **2** in a 1:1 ratio. This method revealed to be strictly necessary, and it was described for the first time by Elder¹⁰² and subsequently successfully applied by Gomes et al.⁶⁹ In fact, the synthesis of the free ligands 5-A-5'-D-H₂saltn should proceed in two subsequent mono-condensation steps of 5-A-salH and 5'-D-salH to tn. However, our attempts to obtain such mono-condensation always failed and similar difficulties have been also reported by others:⁶⁹ reaction of equimolar amounts of salH (or substituted ones) and tn gave invariably the double condensation products, H_2saltn , even when a 4-fold excess of the diamine was used, making this synthetic method useless. Less-reactive ketones (acetophenone, acetylacetonone, etc.) instead of

salH makes possible the isolation of the tridentate proligands HL and then the synthesis of the unsymmetrically-substituted tetradentate ligands and their metal complexes.^{59,114–117} SalH bearing bulky substituents (i.e. *t*Bu) with diamines like 1,2-diaminocyclohexane or *o*-phenylenediamine also is reported to react to give the monocondensation product.¹¹⁸

Table 2 Main infrared peaks as KBr disks and absorption bands in the UV-vis region as chloroform solution (10^{-4} mol L $^{-1}$) for compounds **1** and **2**.

	Infrared peaks (cm $^{-1}$)			UV-visible absorption bands ^b					
	$\nu(\text{NH}_2)$	$\nu(\text{C}=\text{X})$ ^a	$\nu(\text{NO}_2)$	λ_{max}	ν_{max}	ϵ	λ_{max}	ν_{max}	ϵ
1a (NO $_2$)	–	1633	1306						not soluble
1b (Br)	–	1631	–	399	25060	4130	349	28650	4620
1c (H)	–	1653	–	386	25910	3280	331	30210	5510
1d (Me)	–	1633	–	399	25060	2300	345	28990	5620
1e (OMe)	–	1659	–	422 (sh)	23700	2550	369	27100	6830
2a (NO $_2$)	3313, 3257	1640	1312	389	25710	12550			not present
2b (Br)	3326, 3257	1627	–	383	26110	7490			not present
2c (H)	3326, 3255	1629	–	367	27250	7450			not present
2d (Me)	3317, 3276	1639	–	382	26180	7240			not present

^a X = O for compounds **1** and N for compounds **2**; ^b λ_{max} in nm, ν_{max} in cm $^{-1}$, ϵ in L mol $^{-1}$ cm $^{-1}$

As stated above, in the case of salH and tn the monocondensation can be achieved by template effect of nickel(II) in compounds **2** or with other metal ions like copper(II).^{119–121} At this stage, it would be possible to proceed with the sequestration of nickel as [Ni(dmg) $_2$] (Hdmg = dimethylglyoxime) obtaining the free demetallated proligands HL.^{122–125} Anyway, the following reaction with a second differently-substituted salH gave in our hands always small amounts of symmetrically-substituted derivatives, as detected by mass spectrometry, which in our case hampers obtaining pure compounds **3** after reaction with nickel(II) salts.

Due to the unsymmetrical substitution of compounds **3**, their synthesis following Scheme 1 was achieved with two different combinations, depending on whether the substituents A (and D) were carried by derivative **1** or **2**. Then, each compound **3** has two synthetic methods, except for **3c** and **3g**, since **2e** could not be obtained. Also the hypothetical compound with A = NO $_2$ and D = OMe had only one possible combination, **1e** + **2a**, but even after one month under reflux, we could not obtain the desired compound [Ni(5-NO $_2$ -5'-OMe-saltn)] (**3i**) but always recover a mixture of the two starting materials. The reaction times for the different compounds **3** are very different, depending on the substituents and their positions (See Experimental Section). For example, **1a** + **2c**

yielded **3j** in only 5 h, while the mixture **1c** + **2a** needed to be refluxed for 12 h before total conversion in the final product.

View Article Online
DOI: 10.1039/C9DT01216H

Compounds **3a**, **3d** and **3h** with symmetrically-substituted ligands, $[\text{Ni}(5,5'\text{-G}_2\text{-saltn})]$, G = H, Br, NO₂, respectively, were synthesized by a modification of literature procedures,^{77,78} using nickel(II) chloride and the addition of Et₃N to deprotonate the proligands 5,5'-G₂-H₂saltn, obtained in situ without isolation (see Experimental Section). The use of the chloride salt instead of nickel(II) acetate revealed to be necessary since the reaction of 5,5'-G₂-H₂saltn (either previously isolated or in situ) and Ni(AcO)₂·4H₂O in a 1:1 ratio led to the trinuclear derivatives $[\text{Ni}_3(\mu\text{-}5,5'\text{-G}_2\text{-saltn})_2(\mu\text{-AcO})_2]$ (G = NO₂, Br, H).^{78,126–129}

Table 3 Infrared stretching bands (cm⁻¹) and ESI⁺ mass peaks (*m/z*) for compounds **4**.

compound	reaction	G	G'	$\nu(\text{NH}_2)$	$\nu(\text{C=N/C=O})$	<i>m/z</i>
4a	1c + tn	H	H	3344, 3290	1633	–
4b	1d + 2c	H	Me	3348, 3288	1633	235 $[\text{Ni}(\text{HL})]^+$
4b'	1c + 2d	Me	H	3346, 3287	1648, 1634	249 $[\text{Ni}(\text{MeL})]^+$
4e	1c + 2b	Br	H	3342, 3293	1652, 1631	313 $[\text{Ni}(\text{BrL})]^+$
4e'	1b + 2c	H	Br	3349, 3293	1638	235 $[\text{Ni}(\text{HL})]^+$
4f	1d + 2b	Br	Me	3339, 3290	1631	–
4g	1e + 2b	Br	OMe	3341, 3290	1637	–

In some cases, after few hours under reflux of the derivatives **1** and **2**, it was possible to isolate light green compounds whose elemental analyses were close to the ones for the desired products **3**, but still show two NH₂ stretching bands in their infrared spectra. Those bands were at higher wavenumbers compared to complexes **2**, and the C=O or C=N band was also shifted (Table 3), meaning that the starting materials reacted to a different compound, which is not the final product **3**. Furthermore, peaks due to the $[\text{Ni}(\text{GL})]^+$ fragments are still visible in the mass spectra (Table 3), meaning that the condensation has not yet occurred. These intermediates **4** are most probably dinuclear species (Scheme 1) in analogy to what recently reported by Ghosh et al,⁷⁰ formed by scrambling of the ligands ^Gsal⁻ and ^GL⁻ between the two nickel ions of compounds **1** and **2**. Interestingly, from the synthesis of **3a** with the Holm's method⁷⁹ by reaction of $[\text{Ni}(\text{Hsal})_2(\text{H}_2\text{O})_2]$ (**1c**) with tn in a 1:1 ratio under reflux in ethanol for 2 h, we could also isolate the intermediate $[\text{Ni}_2(\mu\text{-HL})_2(\text{Hsal})_2]$ (**4a**), visible in the infrared spectrum by the appearance of the NH₂ stretching bands at higher wavenumbers compared to **2c**, as observed for the other intermediates **4**. It is noteworthy to observe how no intermediates with NO₂ group could be isolated, but compounds **1** and **2** directly scramble their ligands, and condensation to the unsymmetrically-substituted

derivatives **3** occurred on nickel(II) sites immediately after, suggesting an effect due to the electron-withdrawing nature of the substituent.

View Article Online
DOI: 10.1039/C9DT01216H

X-ray crystal structures of **3c**·CHCl₃, **3g**·EtOH and **3j**

Crystals suitable for X-ray structure determination were obtained by slow diffusion of ⁱPr₂O into CHCl₃ (**3c** and **3j**), or *n*-hexane into EtOH (**3g**). Selected bond distances and angles are provided in Table 4, and an ORTEP diagram of their structures with atom numbering scheme is shown in Figs. 1–3. All compounds crystallize in head-to-tail stacked couples to form centrosymmetric pairs.

In **3c**·CHCl₃, the two molecules of the centrosymmetric pair are slightly shifted one with respect to the other, leading to a relatively long Ni···Ni_{1-x,1-y,1-z} distance, 3.7035(4) Å. The shorter interatomic contact within a pair is C5···C17_{1-x,1-y,1-z}, 3.3100(25) Å, while the Ni···N2_{1-x,1-y,1-z} distance, 3.5162(16) Å, is too long to consider the Ni ion in a square-pyramidal coordination. Each centrosymmetric pair interacts with an adjacent one through weaker π···π interactions (shorter contact, C14···C17_{2-x,2-y,1-z}, 3.3681(26) Å), affording a zig-zag motif (Fig. 1). The molecule assumes an almost planar conformation, with a slight deformation towards a saddle shape where the dihedral angle between the least-squares (l.s.) planes through the aromatic rings is 13.6(1)°. The nickel(II) ion resides in a slightly distorted square planar environment, with a maximum deviation from the N₂O₂ l.s. plane equal to 0.003(1) Å. The six-membered chelate ring NiN1C1C2C3N2 assumes approximately a screw-boat conformation ($\varphi = 79.0(2)^\circ$, $\vartheta = 66.9(1)^\circ$), with a total puckering amplitude $Q = 0.617(2)$ Å.^{130,131} The structure is stabilized by a co-crystallized chloroform molecule, hydrogen bonded with both the phenoxido oxygen atoms O1 and O2 (H···O distances, 2.41(1) and 2.19(1) Å, C–H···O angles, 143.1(1) and 155.5(1)°, respectively, Fig. 1).

Table 4 Experimental coordination distances (Å) and angles (°) for **3c**·CHCl₃, **3g**·EtOH and **3j**.

	3c ·CHCl ₃	3g ·EtOH	3j
Ni–O1	1.8489(12)	1.859(3)	1.8573(9)
Ni–O2	1.8501(11)	1.855(3)	1.8446(10)
Ni–N1	1.8971(14)	1.906(4)	1.8757(11)
Ni–N2	1.9115(13)	1.908(4)	1.8679(11)
Ni···Ni ^a	3.7035(4)	3.3632(11)	3.4662(3)
O1–Ni–O2	78.57(5)	78.59(13)	83.94(4)
O1–Ni–N1	92.74(6)	92.18(16)	92.11(4)
O2–Ni–N2	91.81(5)	92.55(14)	92.86(5)
N1–Ni–N2	96.89(6)	96.70(16)	91.46(5)
O2–Ni–N1	171.26(6)	170.73(16)	172.13(5)

O1–Ni–N2	170.36(6)	170.97(15)	175.36(5)
Ni...N ₂ O ₂ ^b	0.003(1)	0.007(2)	0.028(1)

View Article Online
DOI: 10.1039/C9DT01216H

^a symmetry operations are: $1-x, 1-y, 1-z$ (**3c**), $-x, 2-y, -z$ (**3g**) and $1-x, -y, -z$ (**3j**); ^b metal distance from the N₂O₂ l.s. coordination plane.

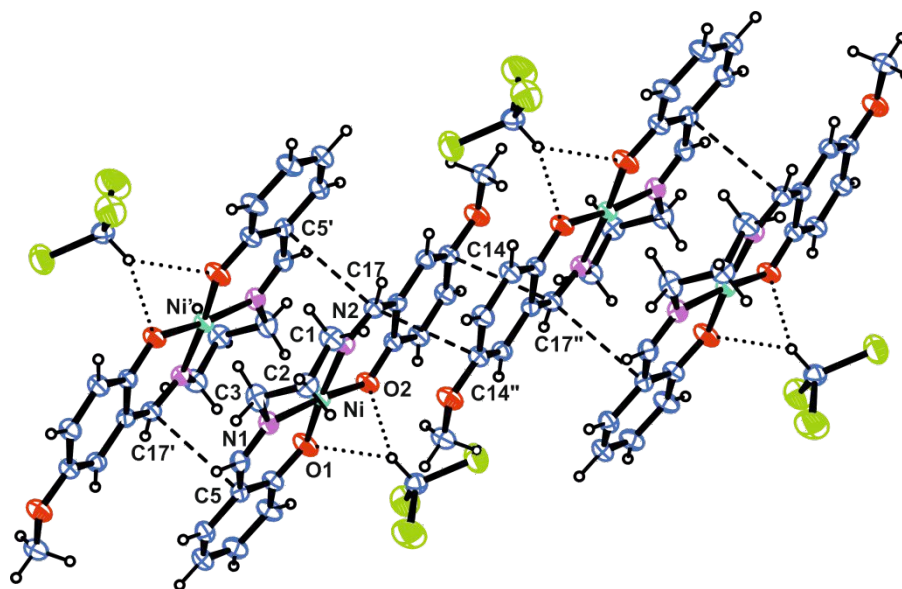


Fig. 1 Stacking of centrosymmetric pairs of molecules in **3c**·CHCl₃ with short intermolecular contacts. Thermal ellipsoids are drawn at 30% probability level. Colour code: Ni = green, Cl = yellow-green, O = red, N = purple, C = blue, H = white.

In compound **3g**·EtOH, the two molecules of the centrosymmetric pair are almost overlapped, giving rise to a relatively short Ni...Ni_{*x,2-y,-z*} distance, 3.3632(11) Å. This packing could be considered responsible for an almost planar conformation of the complex, where the dihedral angle between the l.s. planes through the aromatic rings is 3.3(1)°. The only atoms significantly deviating from the molecular plane are the carbon atoms of the tn chain, which is partially disordered over two positions, A and B (in Fig. 2 only the most populated site, A, is reported). Both the disordered chelate rings assume approximately a twisted conformation ($\varphi = -99.6(5)$ and $79.2(9)^\circ$, $\vartheta = 83.1(4)$ and $98.7(6)^\circ$ for A and B rings, respectively) and are more puckered than the chelate ring of **3c**·CHCl₃ ($Q = 1.78(5)$ and $1.93(9)$ Å, respectively). Adjacent dimers interact through weak C–H...O interactions. The structure is stabilized by a co-crystallized EtOH molecule, whose hydroxyl group forms a bifurcated hydrogen bond with the phenoxido oxygen atoms O1 and O2 (H...O distances, 2.17(1) and 2.55(1) Å, O–H...O angles, 161.3(1) and 112.1(1)°, respectively).

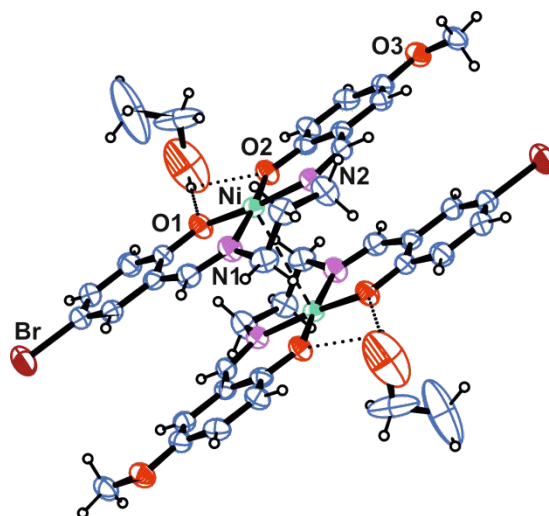


Fig. 2 ORTEP plot of a centrosymmetric pair of **3g**·EtOH with short intermolecular contacts. Thermal ellipsoids are drawn at 30% probability level. Colour code: Br = brown, Ni = green, O = red, N = purple, C = light blue, H = white.

In **3j** (see (Fig. 3), the two molecules of the centrosymmetric pair are slightly shifted one with respect to the other and the shortest intradimeric distance is $C9 \cdots C17_{1-x,-y,-z}$, 3.215(2) Å. The complex assumes a step-like shape, probably as a consequence of the conformation of the tn bridge placing C1 and C3 on either sides with respect to the N_2O_2 plane. The l.s. planes through the two aromatic rings are almost parallel (the dihedral angle between them is equal to $5.0(1)^\circ$) but strongly deviate from the N_2O_2 l.s. plane (the dihedral angles formed by the latter with the C5–C10 and the C11–C16 l.s. planes measure $25.16(3)$ and $27.87(4)^\circ$, respectively). In such a quite distorted conformation, the nickel(II) ion shows a slightly larger deviation from the N_2O_2 l.s. plane ($0.028(1)$ Å) with respect to **3c** and **3g**, towards the oxygen atom O2 of the pair stacked molecule ($Ni \cdots O2_{1-x,-y,-z} = 3.339(1)$ Å). It is worth noting that O2 belongs to the donor sal moiety of the unsymmetrically-substituted saltn ligand. The chelate ring assumes a twisted conformation ($\varphi = 88.4(1)^\circ$, $\vartheta = 90.2(1)^\circ$) with total puckering amplitude $Q = 0.770(1)$ Å, comparable with that of **3c**·CHCl₃.

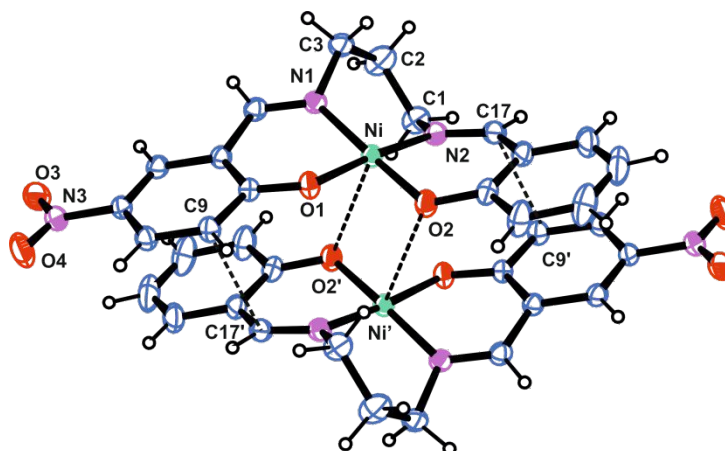


Fig. 3 ORTEP plot of a centrosymmetric pair of **3j** with short intermolecular contacts. Thermal ellipsoids are drawn at 30% probability level. Colour code: Ni = green, O = red, N = purple, C = light blue, H = white.

Optimized Geometries

The coordination bond lengths for all the optimized compounds are reported in Table 5. By looking at the two Ni–O and Ni–N distances obtained for the symmetrically-substituted **3a** (H,H), **3d** (Br,Br) and **3h** (NO₂,NO₂), differing by about 0.010 Å, it appears that these complexes can be intrinsically considered non symmetric from a structural point of view, a feature already pointed out in our previous report on the analogues [Cu(5-A-5'D-saltn)] derivatives³⁸ and observed in the X-ray molecular structures of [Cu(saltn)]^{132,133} but also in some [Ni(saltn)] ones¹³⁴ with unoccupied fifth coordination position. We ascribed such asymmetry to the strain arising from the presence of the three fused six-membered rings, which is mainly relaxed through a widening of the N–Ni–N angle with respect to the O–Ni–O one (clearly observed in both X-ray and optimized structures), but also by the observed non-equivalence of the coordination bond lengths.

Substitution of the A group on the saltn skeleton (compare e.g. **3a** with **3e** and **3j**, or **3b** with **3f** and **3k**, or even **3c** with **3g** and **3l**) influences in a greater extent the Ni–O distances with respect to the Ni–N ones, with almost negligible variations going from H to Br but more important ones from H to NO₂. In particular, addition of the NO₂ group results in an increase of the Ni–O1 and Ni–N1 bond lengths by about 0.010 and 0.006 Å (acceptor side), respectively, and a decrease of the Ni–O2 and Ni–N2 bond lengths by about 0.009 and 0.005 Å (donor side), reflecting the tendency of the nickel(II) ion to move closer to the donating sal moiety. Comparison with the X-ray structures of **3c**, **3g** and **3j** indicates that the coordination bond lengths are satisfactorily reproduced within 0.01 Å with the only exception of the Ni1–N distances of **3j**, which are significantly shorter (by about 0.04 Å) in the experimental geometry with respect to the optimized one. Such discrepancy could be however ascribed to the severely distorted conformation of the X-ray structure of **3j**, as also suggested by comparison with **3c**·CHCl₃ and **3g**·EtOH. In the latter structures not only the

Ni1–N bond lengths are 0.02–0.04 Å longer than those of **3j**, but the O1–Ni–O2 and N1–Ni–N2 angles are respectively greater and smaller by about 5° than those observed in **3j**.

View Article Online
DOI: 10.1039/C9DT01216H

Table 5 Coordination bonds (Å) and angles (°) for the optimized geometries of **3a–3l**.^a

compd.	A	D	Ni–O1	Ni–O2	Ni–N1	Ni–N2	O1–Ni–O2	N1–Ni–N2
3a	H	H	1.854	1.864	1.906	1.917	81.94	94.53
3b	H	Me	1.854	1.863	1.907	1.917	81.98	94.51
3c	H	OMe	1.854	1.862	1.906	1.915	82.04	94.54
3d	Br	Br	1.853	1.864	1.906	1.917	81.98	94.49
3e	Br	H	1.856	1.861	1.908	1.915	81.95	94.55
3f	Br	Me	1.856	1.860	1.908	1.915	81.95	94.54
3g	Br	OMe	1.857	1.859	1.908	1.914	81.99	94.58
3h	NO ₂	NO ₂	1.855	1.866	1.906	1.915	81.75	94.57
3i	NO ₂	Br	1.861	1.858	1.910	1.913	81.86	94.57
3j	NO ₂	H	1.864	1.855	1.912	1.912	81.81	94.63
3k	NO ₂	Me	1.864	1.855	1.912	1.911	81.81	94.61
3l	NO ₂	OMe	1.865	1.853	1.912	1.910	81.84	94.66

^aCalculations performed at M06/6-311++G(d,p) level of theory; O1 and N1 belong to the sal moiety with A group, while O2 and N2 to the sal moiety with D group.

The Ni...N₂O₂ distances, going from 0.026 to 0.031 Å for all optimized structures, are slightly larger than those observed in **3c**·CHCl₃ and **3g**·EtOH, further suggesting some role of the head-to-tail intradimeric stacking on the molecular conformation in the solid state. Such effect is also shown by a more pronounced saddle shape of the optimized geometries. The dihedral angles between the l.s. planes through the aromatic rings of the two sal moieties are in the range 31.33–33.73°, higher than the experimental ones due to the absence of head-to-tail pairs. A modulation given by the donor group side can be observed in the three series **3a–3c** (32.42, 32.32 and 32.22°), **3d–3g** (33.21, 32.40, 32.34 and 31.86°) and **3h–3l** (33.73, 33.19, 32.33, 31.84 and 31.33°) on going from NO₂ to Br, H, Me and OMe.

Experimental and simulated electronic absorption spectra

The electronic spectra of compounds **3** in CHCl₃ at 10⁻⁴ mol L⁻¹ solutions are reported in Fig. 4a in the 10000–35000 cm⁻¹ (1000–285 nm) region, where it can be clearly discerned the distinctive

behaviour of complexes without (**3a**, **3b**, **3c**, **3e**, **3f** and **3g**) and with NO₂ (**3i**, **3j** and **3k**). In fact, the presence of the nitro as acceptor group causes the threefold increase in the intensity of the broad absorption from 20000 to 33300 cm⁻¹ (500–300 nm). This effect can be also observed comparing [Ni(salophen)]⁵¹ with [Ni(4,4'-bis-diethylaminosalo-4,5-dinitro-phen)].⁵⁵ The list of the observed maxima with corresponding molar extinction coefficients, ϵ , are reported in Table 6, where it is possible to recognise mainly two or three absorptions together with shoulders, assignable to the convolution of MLCT and ILCT transitions (see below for further details). The *d-d* transition falls around 16700 cm⁻¹ (600 nm) with very low ϵ (~ 80 L mol⁻¹ cm⁻¹),⁷⁹ which makes very difficult to see it in the absorption spectrum. It has also to be noted that Br as substituent seems to behave as a weak donor group, similar to Me (compare the spectra of **3b** with **3e**, **3c** with **3g** and **3i** with **3k**), rather than a weak acceptor group: this can be clearly seen on going from **3b** to **3f**, where the introduction of Br in the combination (Br,Me) causes only very subtle modification in the absorption spectrum with respect to (H,Me). The same feature can be recognised in derivatives **1** and **2** in Table 2.

Table 6 Absorption bands of compounds **3** in the UV-visible region in CHCl₃ solution (10⁻⁴ mol L⁻¹, optical path = 0.5 cm).^{a,b}

			MLCT			ILCT $\pi \rightarrow \pi^*$			ILCT $\pi \rightarrow \pi^*$		
	A	D	λ_{\max}	ν_{\max}	ϵ	λ_{\max}	ν_{\max}	ϵ	λ_{\max}	ν_{\max}	ϵ
3a	H	H	419	23850	7460	350	28600	8960	316	31650	8030
3b	H	Me	423	23640	5500	351	28490	6530	321	31150	7030
3c	H	OMe	431	23200	5520	357	28010	6750	330sh	30300	5920
3e	Br	H	422	23700	5240	353	28330	6570	322sh	31060	5650
3f	Br	Me	429	23310	5610	354	28250	6240	327sh	30580	5730
3g	Br	OMe	435	22990	5740	357	28010	6030	331	30210	5920
3i	NO ₂	Br	383 ^c	26110	14580	359	27860	15690			
3j	NO ₂	H	382 ^c	26110	17960	358	27930	17770			
3k	NO ₂	Me	381 ^c	26240	15080	361	27700	15890			

^a **3d** and **3h** not soluble; ^b λ_{\max} in nm, ν_{\max} in cm⁻¹, ϵ in L mol⁻¹ cm⁻¹; ^c convolution of MLCT+ILCT

Excitation energy calculations on compounds **3** (see Table S2 in ESI for the transitions with oscillator strength $f > 0.01$) reproduce satisfactorily the trend observed in the absorption spectra, in particular: *i*) it is recognized the presence of three main CT bands (besides the low energy *d-d* transitions); *ii*) the presence of the D group implies systematically a red-shift of the three transitions (compare e.g. **3a** with **3b** and **3c**) while no clear trend could be associated with the presence of the A group; *iii*) introduction of NO₂ leads to an increase of the oscillator strengths for the highest

energy transitions, though not so marked as observed in the experimental spectra. By analysing the major contributions to the transitions, it is confirmed the attribution of the three bands to MLCT (for the lowest energy one) and ILCT (for the two highest energy ones) character, though the contribution of the metal's *d* orbitals to the HOMO is generally quite low (*d* population ≤ 0.11), as also evident by looking at the isodensity surface plots of the frontier orbitals mainly involved in the computed transitions for **3c** and **3j** (see Fig. S1 in the ESI). The MLCT nature of the lowest-lying transition is in agreement with what previously reported for N₂O₂ Schiff base nickel(II) complexes.^{50,54} Nevertheless, the accessibility to ILCT charge transfer transitions with similar energies is in this case present, especially because of the blue-shift of the MLCT band compared to [Ni(salophen)].⁵¹ This fact does confirm the expected effect of the distortion from perfectly square planar geometry around the metal centre induced by the flexibility of the tn bridge between the two sal moieties, as observed from the X-ray molecular structures and confirmed in solution from DFT calculations. For comparison purposes, excitation energy calculations were computed also for two selected analogue copper(II) complexes, namely **Cu3a** and **Cu3l** (see Table S2 in ESI), where the substitution is the same as in the nickel(II) complexes **3a** and **3l**. Interestingly, the complexes **Cu3a** and **Cu3l** reveal the opposite LMCT character of the lower energy band with an enhanced contribution of the metal's *d* orbitals (*d* population about 0.60), in agreement with what previously reported by us with a different DFT approach.³⁸

UV-visible studies at increasing dilutions from 10⁻³ down to 5 × 10⁻⁶ mol L⁻¹ were also performed for **3c** (H,OMe) and **3j** (NO₂,H) in the 20000–35000 cm⁻¹ (500–285 nm) region in order to inspect the presence of aggregation bands due to dimeric units and unambiguously assign the absorption maxima reported in Table 6. In fact, as observed in their X-ray crystal structures, these dipolar molecules tend to couple in head-to-tail pairs, which might survive even at a concentration as low as 10⁻⁴ mol L⁻¹. Furthermore, this aggregation phenomenon is well known for salen-type zinc(II) derivatives,^{135–139} which show dimeric blue-shifted absorption bands that decrease in intensity upon high dilution of the solution down to 10⁻⁶ mol L⁻¹ with the formation of bathochromic-shifted absorptions of the monomeric units.¹³⁵ The results obtained for **3j** and **3c** are reported in Fig 4b and Fig. S2a in the ESI, respectively, and it can be observed that there are only very minor changes in the absorption profile for both complexes, the most notable one being the increase of intensity of the maximum at 358 nm with respect to the one at 383 nm for **3j** (Fig. 4b). This allows us to exclude the presence of aggregation in solution, if not in really minor percentage.

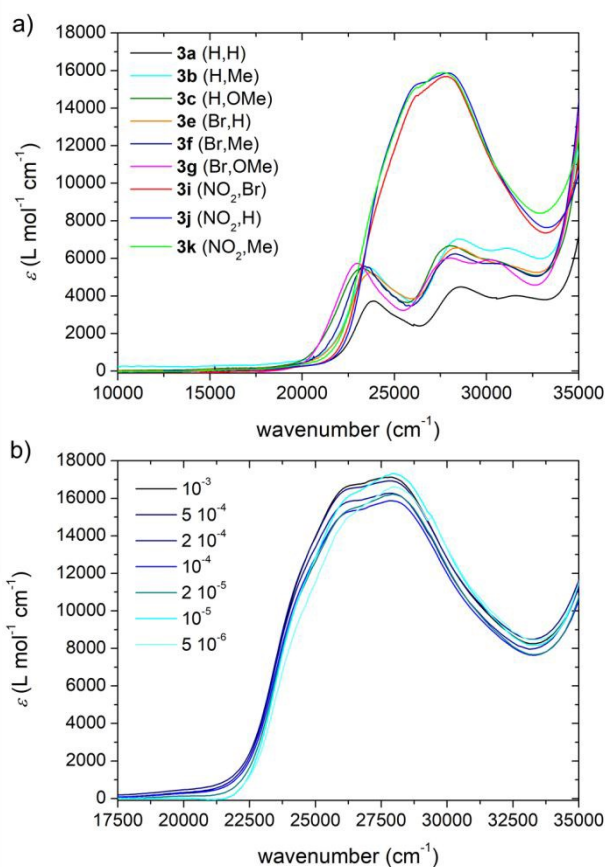


Fig. 4 UV-visible absorption spectra of a) compounds **3** in 10^{-4} mol L $^{-1}$ CHCl $_3$ solutions, and b) dilution studies of **3j** from 10^{-3} down to 5×10^{-6} mol L $^{-1}$ CHCl $_3$ solutions.

An explanation for the observed difference between zinc(II) and nickel(II) complexes can arise from the fact that Zn \cdots O intermolecular interactions are much stronger and more specific with the former metal ion (i.e. 2.05 Å for [Zn(salen)]^{140,141}) than in the case of our nickel(II) derivatives, in which we could observe again short but much longer Ni \cdots O intermolecular contacts only in **3j** (3.339(1) Å) while in the other cases there are non-specific contacts.

Compounds **3c** and **3j** as representatives of the two categories without and with NO $_2$ group, respectively, were also subjected to qualitative solvatochromism studies. For the former compound without nitro group, the MLCT band shows a hypsochromic behaviour on going from 23100 cm $^{-1}$ (433 nm) in the less polar toluene to 24270 cm $^{-1}$ (412 nm) in the most polar MeOH (Fig. S2b in the ESI), with a small but gradual shift with the polarity of the solvents from one extreme to the other. This is in agreement with the computed small decrease (1.41 D) of the dipole moment for its HOMO \rightarrow LUMO transition (see Table S2), which also justifies the absence of hypsochromic shift of the CT band upon addition of increasing amount of DMSO in the CHCl $_3$ solution (Fig. S2c in the ESI). In fact, the MLCT band in pure DMSO is at 23590 cm $^{-1}$ (424 nm), only 7 nm away from the value in pure CHCl $_3$, 23200 cm $^{-1}$ (431 nm).

In the case of **3j**, moving from low-medium polar (toluene, AcOEt, CHCl₃, CH₂Cl₂) to highly polar (CH₃CN, EtOH and MeOH) solvents with the exception of DMSO and DMF, there is a decrease in intensity of the maximum at 27900 cm⁻¹ (358 nm) with a concomitant increase in intensity of the signal at 26100 cm⁻¹ (382 nm) in CHCl₃, together with its bathochromic shift to 25840 cm⁻¹ (387 nm) in MeOH, as it can be observed in Fig. S3a in the ESI. This solvatochromism is opposite to what observed for **3c** and to what highlighted in the previous dilution study, so confirming the absence of stacked pairs in solution. Our data suggest that **3j** should possess an excited state with a higher dipole moment with respect to the ground state, and this is fully consistent with what observed for the analogue copper(II) complexes in the presence of the nitro group.³⁸ Though such band is a convolution of both MLCT (or LMCT in copper(II) complexes) and ILCT bands, its observed red-shift is confirmed by the computed increase (equal to 5.39 D for **3j**) of the dipole moment from the ground to the excited state of the HOMO → LUMO transition.

The behaviour observed in DMF and DMSO, where the MLCT band shows the highest hyperchromic shift (397 and 404 nm, respectively) even if those solvents are not the most polar in the Reichardt scale, could be also caused by the apical interaction of the solvent molecules. To prove this point, we added increasing amount of DMSO to the 10⁻⁴ mol L⁻¹ CHCl₃ solution of **3j** and the results are reported in Fig. S3b in the ESI. The addition of gradually increasing amount of DMSO from 5 up to 200 μL (2800 μmol, 14,000-fold excess) leads the spectrum to an increase in the molar absorptivity especially for the band at higher wavelength, which moves from 382 to 388 nm. The spectrum becomes more similar to the one in pure DMSO, which then suggests that we are observing the combined effect of the increasing polarity of the solvent mixture together with the interaction of the solvent with the nickel(II) centre. The difference observed with **3c** can be reasonably justified by the presence of the electron withdrawing NO₂ group in **3j**, which makes the metal more eager of further donation from surrounding molecules, while the electron donating OMe is sufficient to avoid such an interaction.

NLO properties

The NLO properties of selected [Ni(5-A-5'-D-saltn)] complexes as obtained by EFISH technique are reported in Table 7. EFISH experiments provide the second-order NLO response (β_{vec}) along the μ_g direction, which coincides, in the case of linear or pseudo-linear push-pull molecules, with that of the intramolecular CT transition. In complexes **3**, as previously reported for the analogue copper(II) complexes,³⁸ two main CT directions can be identified, one from the A towards the D groups (approximately, the *x*-axis) and the other from the N₂ towards the O₂ atoms of the donor set (approximately, the *y*-axis), as indeed present in the unsubstituted [Ni(saltn)] (see below). The *z* component of CT, when present, may be neglected on a first approximation because

it derives from the distortion of complexes from planarity and it is therefore strictly connected, in both direction and magnitude, with their conformational flexibility in solution. Therefore, β_{vec} values might not be fully informative about the multiple origin of the NLO response in complexes **3**. Aware of this problem, we are here reporting the EFISH measurements in combination with theoretical calculations, in order to distinguish the different components and compare the NLO response of nickel(II) derivatives **3** with that of the analogue copper(II) ones³⁸ and of all the other nickel(II) compounds with similar N₂O₂ tetradentate Schiff base ligands reported in the literature,^{49–51,53–55,57,58,65,142} mainly analysed by means of EFISH measurements.

Table 7 Second-order EFISH data at 1907 nm of compounds **3** in CHCl₃ solution (error on the experimental $\mu_g\beta_{vec}$ data is about 10%).

compd.	A	D	concentration (mol L ⁻¹)	$\mu_g\beta_{vec}$ ($\times 10^{-30}$ D cm ⁵ esu ⁻¹)	β_{vec}^a ($\times 10^{-30}$ cm ⁵ esu ⁻¹)
3a	H	H	5×10^{-4} , 10^{-4}	610, 820	73, 98
3b	H	Me	5×10^{-4} , 10^{-4}	390, 440	48, 54
3c	H	OMe	5×10^{-4} , 10^{-4}	710, 1050	73, 108
3e	Br	H	5×10^{-4} , 10^{-4}	480, 520	52, 57
3f	Br	Me	5×10^{-4} , 10^{-4}	570, 660	63, 72
3g	Br	OMe	5×10^{-4} , 10^{-4}	580, 670	56, 65
3i	NO ₂	Br	$10^{-4}{}^b$	630 ^b	55 ^b
3j	NO ₂	H	5×10^{-4} , 10^{-4}	520, 820	42, 66
3k	NO ₂	Me	2.5×10^{-4} , 10^{-4}	680, 770	54, 61

^a Extracted using the μ_g values computed on the M06/6-311++G(d,p) optimized geometry at CAM-B3LYP/6-311++G(d,p)/IEFPCM(CHCl₃) level of theory, see Table 8 for complete data; ^b **3i** not soluble enough for the highest concentration.

The measured $\mu_g\beta_{vec}$ quantities are in the same range as that of the corresponding [Cu(5-A-5'-D-saltn)] complexes previously reported³⁸ at the same concentration (400–700 vs. 300–600 $\times 10^{-30}$ D cm⁵ esu⁻¹, respectively, at 5×10^{-4} mol L⁻¹). Measurements on 10^{-4} mol L⁻¹ solutions usually provided slightly larger $\mu_g\beta_{vec}$ values than those obtained at 5×10^{-4} mol L⁻¹. By the way, the observed increase is only about 8–14%, i.e. comparable to the experimental error (10%), with the exception of **3a**, **3c** and **3j** (25–37%). At working concentrations lower than 10^{-4} mol L⁻¹ the EFISH response started to be very weak: measurements at 7×10^{-5} mol L⁻¹ CHCl₃ solution of **3c** and **3j** gave $\mu_g\beta_{vec}$ values equal to 1240 and 900×10^{-30} D cm⁵ esu⁻¹ but with higher error (about 25%). This means that the observed increase of $\mu_g\beta_{vec}$ values does not reflect a real effect of

dilution, in support of the UV-visible spectroscopic studies which suggest discarding the presence of aggregated pairs in solution.

View Article Online
DOI: 10.1039/C9DT01216H

Using the dipole moments computed in CHCl_3 (see Table 8), the β_{vec} values reported in the last column of Table 7 are obtained. Comparison with the values of corresponding copper(II) complexes,³⁸ for the few cases where they are available, i.e. (H,H), (H,OMe) and (NO₂,H), indicates that the NLO response of the nickel(II) complexes is slightly higher than that of copper(II) ones. On the other hand, any systematic trend of the NLO response due to the different A–D substitutions cannot be undoubtedly discerned in either series of complexes.

The dynamical hyperpolarizability tensors $\beta_{1,907}$ of all nickel(II) complexes were also computed in CHCl_3 by means of Coupled-Perturbed (i.e. analytical) techniques in order to shed light on the molecular origin of the NLO response. The results are reported in Table 8 together with the ground state dipole moment μ_{g} and its Cartesian components (see note *a* of Table 8 and Fig. 5 for representative examples with the adopted reference system). Owing to the presence of two CT directions, we also report both quantities β_{vec} and β_{tot} , the latter being the modulus of a “vector” derived from the full β tensor (see note *a* of Table 8 for its definition), together with the Cartesian “components” of β_{tot} . β_{vec} and β_{tot} will coincide (in magnitude) when the CT is unidirectional and oriented along the dipole moment. This situation is depicted by the symmetrically-substituted compounds **3a** (H,H) and **3d** (Br,Br), for which only the *y*-components of both μ_{g} and β_{tot} are significantly different from zero. Interestingly, for **3h** (NO₂,NO₂), while the μ_{y} component is predominant over the *x* and *z* ones, the major component of β_{tot} is along the *z*-axis, even if the distortion degree from planarity of the optimized geometry toward a saddle conformation is similar to that of the other derivatives. This is due to the strong NLO effect played by the NO₂ groups (see also below), which are on the same side with respect to the mean molecular plane, providing a *z*-contribution to β_{tot} . Unfortunately, **3h** is practically insoluble in any organic solvent preventing experimental assessment to this prediction. It is also to be noted that, on account of the different electronic properties of the H, Br and NO₂ substituents, for **3a** and **3d** the two vectors point toward opposite directions, giving rise to a negative β_{vec} projection, while for **3h** they point in the same direction, resulting into a positive β_{vec} projection.

Unsymmetrical substitution on either side of the complexes ‘activates’ in a variable extent the *x* component of μ_{g} and β_{tot} vectors, tilting their direction with respect to the *y* axis, and with the major effect associated with the NO₂ group. In particular, the presence of this group generates a large β_{x} component which prevails on the β_{y} one generating a positive β_{vec} projection, which is otherwise negative (see Table 8 and Fig. 5 for the value of the angle θ between the two vectors μ_{g} and β_{tot}). Moreover, introduction of Me or OMe donor group does not affect significantly the μ_{x}

component but strongly increase β_x (compare **3b**, **3c** with **3a** or **3f**, **3g** with **3e** or even **3k**, **3l** with **3j**).

View Article Online
DOI: 10.1039/C9DT01216H

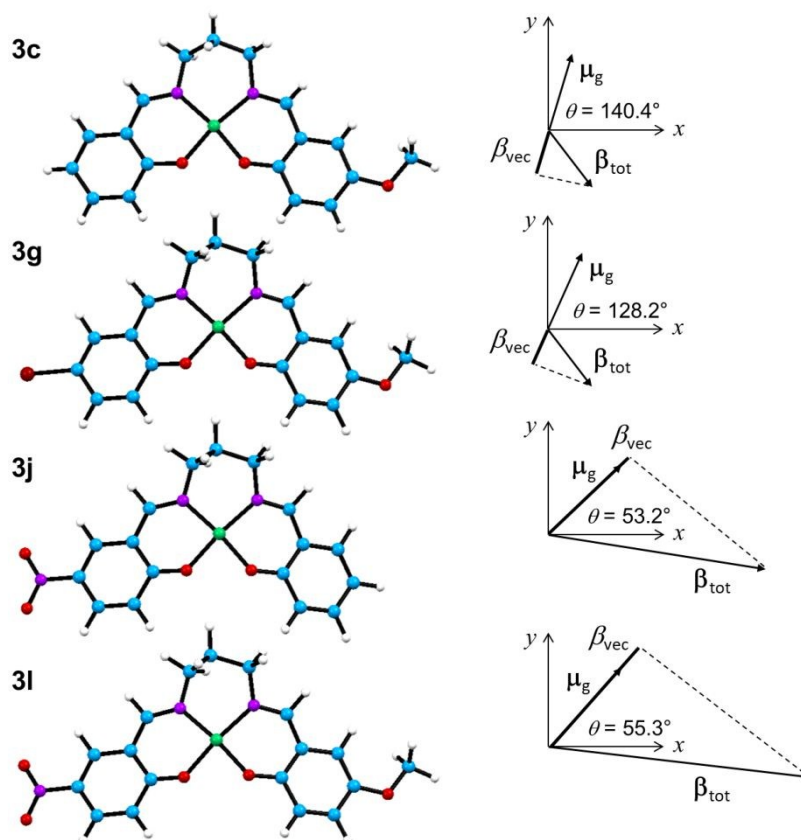


Fig. 5 Directions of the computed μ_g and β_{tot} vectors in the xy Cartesian plane (z axis going inside to complete the right-handed coordinate system), and projection of the latter along the direction of the former, β_{vec} , together with the plot of the optimised geometries for **3c**, **3g**, **3j** and **3l** (colour code: Br = brown, Ni = green, O = red, N = purple, C = blue, H = white).

For comparison purposes, the μ_g and β_{tot} vectors were also computed for four selected analogue copper(II) complexes, namely **Cu3a**, **Cu3c**, **Cu3j** and **Cu3l**, where the A–D substitution is the same as in the nickel(II) complexes **3a**, **3c**, **3j** and **3l**, at the same level of theory as for the nickel(II) ones. It should be first noted that the reduced z -component of both μ_g and β_{tot} vectors in the copper(II) complexes is due to their lower distortion from planarity. This is the result of the increased Cu–O(N) bond lengths compared to the Ni–O(N) ones and the consequent reduced strain associated with the presence of the three six-membered fused rings. As for the x and y components, it is observed that those of the dipole moments do not undergo significant variations going from the corresponding nickel(II) to copper(II) complexes. On the other hand, the β_y component systematically increases from Ni to Cu, while the β_x one is dependent on the nature of the

substituents, increasing for the (H,OMe) complex, decreasing for the (NO₂,H) one and remaining essentially unchanged for the (H,H) and (NO₂,OMe) derivatives.

View Article Online
DOI: 10.1039/C9DT01216H

Table 8 Computed dipole moments (μ_g , μ_x , μ_y and μ_z , D), SHG ($\lambda = 1907$ nm) hyperpolarizabilities (β_{tot} , β_x , β_y and β_z , 10^{-30} cm⁵ esu⁻¹) in CHCl₃ and angle (θ , °) between μ_g and β_{tot} vectors for **3a–l** and selected analogue copper(II) complexes **Cu3x** ($x = \mathbf{a, c, j, l}$).^a

compd.	A	D	μ_g	μ_x	μ_y	μ_z	β_{tot}	β_x	β_y	β_z	β_{vec}	θ
3a	H	H	8.36	0.23	8.16	1.81	8.6	0.9	-8.0	-3.1	-8.4	167.6
3b	H	Me	8.12	0.32	7.84	2.10	10.0	3.9	-8.7	-3.0	-9.1	155.5
3c	H	OMe	9.76	0.32	9.37	2.72	13.5	8.2	-10.5	-2.4	-10.4	140.4
3d	Br	Br	9.13	0.27	8.94	1.81	10.3	1.2	-9.3	-4.1	-9.9	164.0
3e	Br	H	9.18	4.03	8.06	1.76	9.3	-1.0	-8.6	-3.4	-8.7	159.3
3f	Br	Me	9.12	4.20	7.81	2.13	10.5	1.5	-49.2	-3.3	-8.3	142.2
3g	Br	OMe	10.34	4.19	9.12	2.48	13.1	6.1	-11.3	-2.3	-8.1	128.2
3h	NO ₂	NO ₂	11.28	0.42	11.24	-0.74	20.5	2.9	7.5	-18.9	8.8	64.6
3i	NO ₂	Br	11.39	4.98	10.23	0.67	45.9	44.6	0.5	-10.9	19.3	65.1
3j	NO ₂	H	12.48	9.07	8.51	1.02	44.6	43.5	-6.3	-7.5	26.7	53.2
3k	NO ₂	Me	12.66	9.16	8.65	1.21	48.5	47.6	-4.7	-8.4	30.4	51.2
3l	NO ₂	OMe	13.65	9.12	10.06	1.39	53.3	52.4	-5.2	-8.5	30.3	55.3
Cu3a	H	H	8.41	0.00	8.41	0.27	12.7	1.0	-12.6	0.0	-12.6	172.8
Cu3c	H	OMe	9.42	0.06	9.40	-0.71	18.6	11.7	-14.4	-3.7	-14.3	140.2
Cu3j	NO ₂	H	12.65	9.12	8.76	0.35	41.1	39.4	-11.8	1.1	20.3	60.4
Cu3l	NO ₂	OMe	13.82	9.22	10.28	-0.65	54.8	53.4	-12.4	-0.7	26.4	61.2

^a Calculations performed on the M06/6-311++G(d,p) optimized geometry at (CP)CAM-B3LYP/6-311++G(d,p)/IEFPCM(CHCl₃) level of theory. Unrestricted formalism used for copper(II) complexes. The μ_i and β_i components are defined according to the following convention, based on the Gaussian 'standard orientation' and uniformed for comparison purposes: the x and y axes lie on the molecular plane, with x placed in the direction of the largest extension of the molecule, pointing from the acceptor to the donor group, and y pointing from the O₂ to the N₂ atoms of the donor set; the z axis is approximately normal to the N₂O₂ plane, completing the right-handed reference system). Hyperpolarizability is defined as $\beta_{\text{tot}} = (\beta_x^2 + \beta_y^2 + \beta_z^2)^{1/2}$ and $\beta_{\text{vec}} = \sum_i (\mu_i \beta_i) / |\mu|$

where $\beta_i = (1/3)\sum(\beta_{ij} + \beta_{ji} + \beta_{ji})$.¹⁵ In particular $\beta_{\text{tot}} = (5/3)\beta_{\parallel}$ and $\beta_{\text{vec}} = (5/3)\beta_{\parallel}(z)$ where β_{\parallel} and $\beta_{\parallel}(z)$ are the quantities printed in the Gaussian16 output according to the Taylor convention.¹⁴⁹

Comparison between computed and measured β_{vec} values shows a disagreement in the sign for the less polar compounds (**3a–g**) for which the EFISH values are always positive. This result was already reported for the copper(II) derivatives for which another DFT approach (ROB3LYP/6-311++G** in vacuo calculations using the finite-field method) was adopted.³⁸ Since the sign of β_{vec} is determined by the relative predominance of the x (positive β_{vec}) over the y component (negative β_{vec}) of CT, it can be understood that the final result is ultimately determined by a fine calibration of both terms. It can be therefore hypothesized that, on one side, the adopted theoretical approaches suffer from neglecting or incorrectly treating some important contributions to hyperpolarizability, such as vibrations, dispersion and solvation.^{143–146} On the other side, since β_{CT} values derived from solvatochromic measurements of **3c** (negative β_{CT}) and **3j** (positive β_{CT}), besides those previously obtained for copper(II) derivatives,³⁸ follow the same trend as the computed values, it is recognized that hyperpolarizability values strongly relies on the adopted experimental technique. It is also to be mentioned that the recently reported hypsochromic shift of the CT transition in **3a** with increasing polarity of the solvent¹⁴⁸ confirms a negative β_{CT} component for the less-polar derivatives, as here determined. Moreover, even if the two-state model¹⁴⁷ could not be applied for these compounds, showing several CT transitions, it is evident that for **3c** most transitions have small or negative variations of the dipole moment, while for **3j** only positive and large variations are observed.

Literature data available on nickel(II) complexes with similar tetradentate N_2O_2 Schiff base ligands can be roughly divided into two categories: *i*) compounds in which the donor and acceptor groups have a metal-free nature (i.e. NO_2 , CN, Cl, OMe, NEt_2 , etc.) and the NLO properties in solution were mainly measured by EFISH technique,^{49–51,53–55,57,142} and *ii*) compounds in which the donor group is mainly ferrocene while the acceptor group ranges from the NO_2 group to the positively-charged ruthenocene-like fragment, and the NLO measurements were performed with Harmonic Light Scattering (HLS) technique.^{59,61,62,114,115,150–152} The present work can be then considered more related to the first group of compounds, for which the reported second-order efficiencies are in line with our data. Nevertheless, the introduction of organometallic push-pull fragments has widened the modulation possibilities, especially from a switching point-of-view.²⁹

Conclusions

Nickel(II) complexes **3a–l** with unsymmetrically-substituted A–D salt ligands could be suitably obtained by selecting and applying the proper template synthesis,^{69,102} which avoids the contamination with the symmetrical derivatives. The electronic nature of the substituents revealed also to be able to promote or impede the reaction conditions. The flexibility of the propylene bridge between the two salicylaldimine units in the final compounds **3** shows itself in the structural diversity of the molecular structures obtained through single-crystal X-ray diffraction studies of **3c** (H,OMe), **3g** (Br,OMe) and **3j** (NO₂,H), as well as in the DFT-optimized structures, for which the choice of the appropriate starting point revealed to be critical in the final geometry. In particular, distortion around the nickel(II) centre is able to partially relieve the strain arising from the presence of the three fused six-membered metallacycles, and such saddle-shaped geometry is expected to be the most stable in solution.

Changing the metal centre from open-shell d^9 copper(II) to closed-shell d^8 nickel(II) led to a switch of the charge transfer transition from a pronounced ligand-to-metal character for the former³⁸ to a metal-to-ligand band. Distortion of the coordination, higher in the case of nickel(II) with respect to copper(II), causes the presence of energetically low-lying states close to the MLCT transition, which can contribute to the NLO response. By the way, the effect of the substituents, and especially the presence of NO₂, is the noteworthy increase of the CT and hence the NLO efficiency, as depicted by theoretical calculations. Furthermore, the reciprocal arrangement of the electron acceptor A and donor D groups on the organic skeleton modulates both the intensity and the directions of μ_g and β_{tot} vectors, as observed for copper(II) analogues.³⁸

β_{vec} values through EFISH measurements set around $50\text{--}110 \times 10^{-30} \text{ cm}^5 \text{ esu}^{-1}$. These values represent a fraction of the total hyperpolarizability in some instances, especially when NO₂ is present, due to the non-coincidence of the directions of μ_g and β_{tot} . Taking into account the θ angle between the two vectors (Table 8) the experimental β_{vec} value of **3j** (NO₂,H), for example, would derive from a β_{tot} of about $110 \times 10^{-30} \text{ cm}^5 \text{ esu}^{-1}$ ($\beta_{vec} = \beta_{tot} \cos\theta$), an almost double value compared to the fraction sampled with the EFISH technique. A similar estimation of β_{tot} can be extended to all derivatives, which seems to balance the SHG efficiency to about $100\text{--}150 \times 10^{-30} \text{ cm}^5 \text{ esu}^{-1}$. As stated above, this can derive from the use of the EFISH technique, which might flatten the NLO responses, regardless the A–D substitution. Anyway, due to the fine tuning given by the wide range and position of the substituents as highlighted by computed values, the second-order NLO efficiency of both copper(II) and nickel(II) salen-type complexes can be considered promising, and this will be object of our future research, especially by exploring further experimental measurements of the NLO features in order to ascertain the full potentiality of these compounds.

Conflicts of interest

There are no conflicts to declare.

Acknowledgements

This work has been supported by the Italian Ministero dell'Istruzione, dell'Università e della Ricerca (MIUR). The authors thank Mr. Paolo Mercandalli for some experimental work.

References

- 1 P. N. Prasad and D. J. Williams, *Introduction to nonlinear optical effects in molecules and polymers*, Wiley, New York, 1991.
- 2 S. R. Marder, J. E. Sohn and G. D. Stucky, Eds., *Materials for nonlinear optics: chemical perspectives*, American Chemical Society, Washington, DC, 1991.
- 3 M. G. Kuzyk, M. Eich, R. A. Norwood and Society of Photo-optical Instrumentation Engineers, Eds., *Linear and nonlinear optics of organic materials III: 4-6 August, 2003, San Diego, California, USA*, SPIE, Bellingham, Wash, 2003.
- 4 M. G. Papadopoulos, A. J. Sadlej and J. Leszczynski, Eds., *Non-linear optical properties of matter: from molecules to condensed phases*, Springer, Dordrecht, 2006.
- 5 R. W. Boyd, *Nonlinear optics*, Academic Press, Amsterdam ; Boston, 3rd ed., 2008.
- 6 N. Kamanina, Ed., *Nonlinear Optics*, InTech, 2012.
- 7 M. Wakaki, *Optical materials and applications*, CRC Press, Boca Raton, FL, 2013.
- 8 B. Chen and G. Qian, Eds., *Metal-Organic Frameworks for Photonics Applications*, Springer Berlin Heidelberg, Berlin, Heidelberg, 2014, vol. 157.
- 9 P. A. Franken, A. E. Hill, C. W. Peters and G. Weinreich, *Phys. Rev. Lett.*, 1961, **7**, 118–119.
- 10 T. H. Maiman, *Nature*, 1960, **187**, 493–494.
- 11 R. J. Collins, D. F. Nelson, A. L. Schawlow, W. Bond, C. G. B. Garrett and W. Kaiser, *Phys. Rev. Lett.*, 1960, **5**, 303–305.
- 12 M. G. Kuzyk, K. D. Singer and G. I. Stegeman, *Adv. Optics Photon.*, 2013, **5**, 4.
- 13 E. Garmire, *Optics Express*, 2013, **21**, 30532.
- 14 M. G. Kuzyk, *J. Mater. Chem.*, 2009, **19**, 7444.
- 15 D. R. Kanis, M. A. Ratner and T. J. Marks, *Chem. Rev.*, 1994, **94**, 195–242.
- 16 J. A. Delaire and K. Nakatani, *Chem. Rev.*, 2000, **100**, 1817–1846.
- 17 M. J. Cho, D. H. Choi, P. A. Sullivan, A. J. P. Akelaitis and L. R. Dalton, *Progr. Polym. Sci.*, 2008, **33**, 1013–1058.
- 18 L. R. Dalton, P. A. Sullivan and D. H. Bale, *Chem. Rev.*, 2010, **110**, 25–55.
- 19 L. Beverina and G. A. Pagani, *Acc. Chem. Res.*, 2014, **47**, 319–329.
- 20 A. Qin and B. Z. Tang, *Nat. Mater.*, 2014, **13**, 917–918.
- 21 H. Kang, A. Facchetti, H. Jiang, E. Cariati, S. Righetto, R. Ugo, C. Zuccaccia, A. Macchioni, C. L. Stern, Z. Liu, S.-T. Ho, E. C. Brown, M. A. Ratner and T. J. Marks, *J. Am. Chem. Soc.*, 2007, **129**, 3267–3286.
- 22 O. Mongin, L. Porrès, M. Charlot, C. Katan and M. Blanchard-Desce, *Chem. Eur. J.*, 2007, **13**, 1481–1498.

- 23 M. Rodríguez, G. Ramos-Ortíz, J. L. Maldonado, V. M. Herrera-Ambriz, O. Domínguez, R. Santillan, N. Farfán and K. Nakatani, *Spectrochim. Acta A: Mol. Biol. Spectr.*, 2011, **79**, 1757–1761. DOI: 10.1039/C9DT01216H
- 24 J. Heck, S. Dabek, T. Meyer-Friedrichsen and H. Wong, *Coord. Chem. Rev.*, 1999, **190–192**, 1217–1254.
- 25 S. Di Bella, *Chem. Soc. Rev.*, 2001, **30**, 355–366.
- 26 C. Andraud and O. Maury, *Eur. J. Inorg. Chem.*, 2009, **2009**, 4357–4371.
- 27 L. Rigamonti, *La Chimica & l'Industria*, 2010, **Aprile**, 118–122.
- 28 M. G. Humphrey, T. Schwich, P. J. West, M. P. Cifuentes and M. Samoc, in *Comprehensive Inorganic Chemistry II*, Elsevier, 2013, pp. 781–835.
- 29 P. G. Lacroix, I. Malfant and C. Lepetit, *Coord. Chem. Rev.*, 2016, **308**, 381–394.
- 30 S. Kaur, M. Kaur, P. Kaur, K. Clays and K. Singh, *Coord. Chem. Rev.*, 2017, **343**, 185–219.
- 31 X. Liu, C. Manzur, N. Novoa, S. Celedón, D. Carrillo and J.-R. Hamon, *Coord. Chem. Rev.*, 2018, **357**, 144–172.
- 32 M. S. Kodikara, R. Stranger and M. G. Humphrey, *Coord. Chem. Rev.*, 2018, **375**, 389–409.
- 33 M. G. Humphrey, *Aus. J. Chem.*, 2018, **71**, 731–742.
- 34 S. Di Bella, A. Colombo, C. Dragonetti, S. Righetto and D. Roberto, *Inorganics*, 2018, **6**, 133.
- 35 N. Tancrez, C. Feuvrie, I. Ledoux, J. Zyss, L. Toupet, H. Le Bozec and O. Maury, *J. Am. Chem. Soc.*, 2005, **127**, 13474–13475.
- 36 B. Babgi, L. Rigamonti, M. P. Cifuentes, T. C. Corkery, M. D. Randles, T. Schwich, S. Petrie, R. Stranger, A. Teshome, I. Asselberghs, K. Clays, M. Samoc and M. G. Humphrey, *J. Am. Chem. Soc.*, 2009, **131**, 10293–10307.
- 37 L. Rigamonti, B. Babgi, M. P. Cifuentes, R. L. Roberts, S. Petrie, R. Stranger, S. Righetto, A. Teshome, I. Asselberghs, K. Clays and M. G. Humphrey, *Inorg. Chem.*, 2009, **48**, 3562–3572.
- 38 L. Rigamonti, F. Demartin, A. Forni, S. Righetto and A. Pasini, *Inorg. Chem.*, 2006, **45**, 10976–10989.
- 39 D. Roberto, R. Ugo, S. Bruni, E. Cariati, F. Cariati, P. Fantucci, I. Invernizzi, S. Quici, I. Ledoux and J. Zyss, *Organometallics*, 2000, **19**, 1775–1788.
- 40 B. J. Coe, *Chem. Eur. J.*, 1999, **5**, 2464–2471.
- 41 I. Asselberghs, K. Clays, A. Persoons, A. M. McDonagh, M. D. Ward and J. A. McCleverty, *Chem. Phys. Lett.*, 2003, **368**, 408–411.
- 42 B. J. Coe, J. A. Harris, L. A. Jones, B. S. Brunshwig, K. Song, K. Clays, J. Garín, J. Orduna, S. J. Coles and M. B. Hursthouse, *J. Am. Chem. Soc.*, 2005, **127**, 4845–4859.
- 43 B. J. Coe, S. P. Foxon, E. C. Harper, M. Helliwell, J. Raftery, C. A. Swanson, B. S. Brunshwig, K. Clays, E. Franz, J. Garín, J. Orduna, P. N. Horton and M. B. Hursthouse, *J. Am. Chem. Soc.*, 2010, **132**, 1706–1723.
- 44 P. G. Lacroix, I. Malfant, J.-A. Real and V. Rodriguez, *Eur. J. Inorg. Chem.*, 2013, **2013**, 615–627.
- 45 S. Du and H. Zhang, in *Metal-Organic Frameworks for Photonics Applications*, eds. B. Chen and G. Qian, Springer Berlin Heidelberg, Berlin, Heidelberg, 2013, vol. 157, pp. 145–165.
- 46 L. R. Mingabudinova, V. V. Vinogradov, V. A. Milichko, E. Hey-Hawkins and A. V. Vinogradov, *Chem. Soc. Rev.*, 2016, **45**, 5408–5431.

- 47 C. R. Nayar and R. Ravikumar, *J. Coord. Chem.*, 2014, **67**, 1–16.
- 48 P. G. Lacroix, *Eur. J. Inorg. Chem.*, 2001, **2001**, 339–348.
- 49 S. Di Bella and I. Fragalà, *Synth. Metals*, 2000, **115**, 191–196.
- 50 S. Di Bella, I. Fragalà, I. Ledoux, M. A. Diaz-Garcia, P. G. Lacroix and T. J. Marks, *Chem. Mater.*, 1994, **6**, 881–883.
- 51 S. Di Bella, I. Fragalà, I. Ledoux and T. J. Marks, *J. Am. Chem. Soc.*, 1995, **117**, 9481–9485.
- 52 S. Di Bella, I. Fragalà, T. J. Marks and M. A. Ratner, *J. Am. Chem. Soc.*, 1996, **118**, 12747–12751.
- 53 P. G. Lacroix, S. Di Bella and I. Ledoux, *Chem. Mater.*, 1996, **8**, 541–545.
- 54 S. Di Bella, I. Fragalà, I. Ledoux, M. A. Diaz-Garcia and T. J. Marks, *J. Am. Chem. Soc.*, 1997, **119**, 9550–9557.
- 55 F. Averseng, P. G. Lacroix, I. Malfant, G. Lenoble, P. Cassoux, K. Nakatani, I. Maltey-Fanton, J. A. Delaire and A. Aukauloo, *Chem. Mater.*, 1999, **11**, 995–1002.
- 56 F. Averseng, P. G. Lacroix, I. Malfant, N. Périssé, C. Lepetit and K. Nakatani, *Inorg. Chem.*, 2001, **40**, 3797–3804.
- 57 S. Di Bella, I. Fragalà, I. Ledoux and J. Zyss, *Chem. Eur. J.*, 2001, **7**, 3738–3743.
- 58 J. Gradinaru, A. Forni, V. Druta, F. Tessore, S. Zecchin, S. Quici and N. Garbalau, *Inorg. Chem.*, 2007, **46**, 884–895.
- 59 A. Trujillo, M. Fuentealba, D. Carrillo, C. Manzur, I. Ledoux-Rak, J.-R. Hamon and J.-Y. Saillard, *Inorg. Chem.*, 2010, **49**, 2750–2764.
- 60 S. Di Bella, I. P. Oliveri, A. Colombo, C. Dragonetti, S. Righetto and D. Roberto, *Dalton Trans.*, 2012, **41**, 7013–7016.
- 61 S. Celedón, V. Dorcet, T. Roisnel, A. Singh, I. Ledoux-Rak, J.-R. Hamon, D. Carrillo and C. Manzur, *Eur. J. Inorg. Chem.*, 2014, **2014**, 4984–4993.
- 62 N. Novoa, T. Roisnel, P. Hamon, S. Kahlal, C. Manzur, H. M. Ngo, I. Ledoux-Rak, J.-Y. Saillard, D. Carrillo and J.-R. Hamon, *Dalton Trans.*, 2015, **44**, 18019–18037.
- 63 D. Vitalini, P. Mineo, S. Di Bella, I. Fragalà, P. Maravigna and E. Scamporrino, *Macromolecules*, 1996, **29**, 4478–4485.
- 64 E. Scamporrino, S. Bazzano, D. Vitalini and P. Mineo, *Macromol. Rapid Commun.*, 2003, **24**, 236–241.
- 65 J. P. Costes, J. F. Lamère, C. Lepetit, P. G. Lacroix, F. Dahan and K. Nakatani, *Inorg. Chem.*, 2005, **44**, 1973–1982.
- 66 F. A. Cotton, *Advanced Inorganic chemistry*, Wiley, India, 2008.
- 67 J. Zhang, C. Zhong, X. Zhu, H.-L. Tam, K.-F. Li, K.-W. Cheah, W.-Y. Wong, W.-K. Wong and R. A. Jones, *Polyhedron*, 2013, **49**, 121–128.
- 68 P. G. Lacroix, F. Averseng, I. Malfant and K. Nakatani, *Inorg. Chim. Acta*, 2004, **357**, 3825–3835.
- 69 L. Gomes, E. Pereira and B. de Castro, *J. Chem. Soc., Dalton Trans.*, 2000, 1373–1379.
- 70 P. Mahapatra, S. Ghosh, S. Giri and A. Ghosh, *Polyhedron*, 2016, **117**, 427–436.
- 71 C. Reichardt, *Angew. Chem. Int. Ed. Engl.*, 1979, **18**, 98–110.
- 72 J.-L. M. Abboud and R. Notari, *Pure Appl. Chem.*, 1999, **71**, 645–718.
- 73 C. Reichardt and T. Welton, *Solvents and solvent effects in organic chemistry*, Wiley-VCH, Weinheim, Germany, 4th, updated and enl. ed edn., 2011.
- 74 G. C. Percy and D. A. Thornton, *J. Inorg. Nucl. Chem.*, 1973, **35**, 2719–2726.

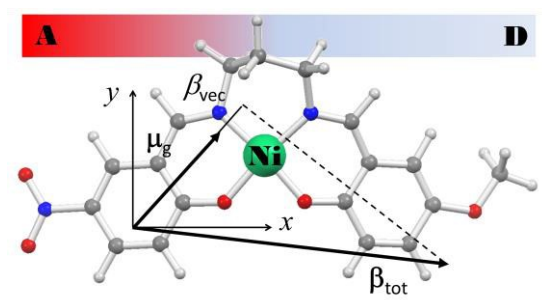
View Article Online
DOI: 10.1039/C9DT01216H

- 75 J. B. Hodgson and G. C. Percy, *Spectrochim. Acta A: Mol. Spectr.*, 1978, **34**, 777–780. New Article Online
DOI: 10.1039/C9DT01216H
- 76 S. Wu and S. Lu, *J. Mol. Cat. A: Chem.*, 2003, **198**, 29–38.
- 77 A. Elmali, C. T. Zeyrek, Y. Elerman and I. Svoboda, *Acta Crystallogr. C*, 2000, **56**, 1302–1304.
- 78 O. Atakol, S. Durmus, Z. Durmus, C. Arici and B. Çiçek, *Synth. React. Inorg. Met.-Org. Chem.*, 2001, **31**, 1689–1704.
- 79 R. H. Holm, *J. Am. Chem. Soc.*, 1960, **82**, 5632–5636.
- 80 Bruker, SMART, SAINT and SADABS, Bruker AXS Inc., Madison, Wisconsin, USA, 1997, .
- 81 G. M. Sheldrick, *Acta Crystallogr. C*, 2015, **71**, 3–8.
- 82 L. J. Farrugia, *J. Appl. Crystallogr.*, 2012, **45**, 849–854.
- 83 M. N. Burnett and C. K. Johnson, *ORTEP-III: Oak Ridge Thermal Ellipsoid Plot Program for crystal structure illustrations*, 1996.
- 84 C. Lee, W. Yang and R. G. Parr, *Phys. Rev. B*, 1988, **37**, 785–789.
- 85 A. D. Becke, *J. Chem. Phys.*, 1993, **98**, 5648–5652.
- 86 S. H. Vosko, L. Wilk and M. Nusair, *Can. J. Phys.*, 1980, **58**, 1200–1211.
- 87 Y. Zhao and D. G. Truhlar, *Theor. Chem. Acc.*, 2008, **120**, 215–241.
- 88 M. Ernzerhof and G. E. Scuseria, *J. Chem. Phys.*, 1999, **110**, 5029–5036.
- 89 C. Adamo and V. Barone, *J. Chem. Phys.*, 1999, **110**, 6158–6170.
- 90 L. E. Johnson, L. R. Dalton and B. H. Robinson, *Acc. Chem. Res.*, 2014, **47**, 3258–3265.
- 91 D. Jacquemin, E. A. Perpète, G. E. Scuseria, I. Ciofini and C. Adamo, *J. Chem. Theory Comput.*, 2008, **4**, 123–135.
- 92 D. Jacquemin, V. Wathelet, E. A. Perpète and C. Adamo, *J. Chem. Theory Comput.*, 2009, **5**, 2420–2435.
- 93 D. Jacquemin, A. Planchat, C. Adamo and B. Mennucci, *J. Chem. Theory Comput.*, 2012, **8**, 2359–2372.
- 94 T. Yanai, D. P. Tew and N. C. Handy, *Chem. Phys. Lett.*, 2004, **393**, 51–57.
- 95 G. Scalmani and M. J. Frisch, *J. Chem. Phys.*, 2010, **132**, 114110.
- 96 M. J. Frisch, G. W. Trucks, H. B. Schlegel, G. E. Scuseria, M. A. Robb, J. R. Cheeseman, G. Scalmani, V. Barone, G. A. Petersson, H. Nakatsuji, X. Li, M. Caricato, A. V. Marenich, J. Bloino, B. G. Janesko, R. Gomperts, B. Mennucci, H. P. Hratchian, J. V. Ortiz, A. F. Izmaylov, J. L. Sonnenberg, D. Williams-Young, F. Ding, F. Lipparini, F. Egidi, J. Goings, B. Peng, A. Petrone, T. Henderson, D. Ranasinghe, V. G. Zakrzewski, J. Gao, N. Rega, G. Zheng, W. Liang, M. Hada, M. Ehara, K. Toyota, R. Fukuda, J. Hasegawa, M. Ishida, T. Nakajima, Y. Honda, O. Kitao, H. Nakai, T. Vreven, K. Throssell, J. A. Montgomery, Jr., J. E. Peralta, F. Ogliaro, M. J. Bearpark, J. J. Heyd, E. N. Brothers, K. N. Kudin, V. N. Staroverov, T. A. Keith, R. Kobayashi, J. Normand, K. Raghavachari, A. P. Rendell, J. C. Burant, S. S. Iyengar, J. Tomasi, M. Cossi, J. M. Millam, M. Klene, C. Adamo, R. Cammi, J. W. Ochterski, R. L. Martin, K. Morokuma, O. Farkas, J. B. Foresman, and D. J. Fox, *Gaussian 16, Revision A.03*, Gaussian, Inc., Wallingford, CT, USA, 2016.
- 97 G. N. Tyson and S. C. Adams, *J. Am. Chem. Soc.*, 1940, **62**, 1228–1229.
- 98 J. M. Stewart, E. C. Lingafelter and J. D. Breazeale, *Acta Crystallogr.*, 1961, **14**, 888–891.
- 99 R. H. Holm, *J. Am. Chem. Soc.*, 1961, **83**, 4683–4690.
- 100 J. Chakraborty, M. Nandi, H. Mayer-Figge, W. S. Sheldrick, L. Sorace, A. Bhaumik and P. Banerjee, *Eur. J. Inorg. Chem.*, 2007, **2007**, 5033–5044.
- 101 M. N. Tahir, D. Ülkü, H. Nazir and O. Atakol, *Acta Crystallogr. C*, 1997, **53**, 181–183.

- 102 R. C. Elder, *Aus. J. Chem.*, 1978, **31**, 35–45.
- 103 C. Sousa, C. Freire and B. De Castro, *J. Coord. Chem.*, 2001, **54**, 1–12.
- 104 C. Sousa, P. Gameiro, C. Freire and B. de Castro, *Polyhedron*, 2004, **23**, 1401–1408.
- 105 M. Di Vaira and P. Orioli, *Inorg. Chem.*, 1967, **6**, 490–495.
- 106 C. R. Choudhury, S. Dey, N. Mondal, S. Mitra, S. O. Ghodsi Mahalli and K. M. Abdul Malik, *J. Chem. Crystallogr.*, 2001, **31**, 57–62.
- 107 Y.-J. Wei, *Acta Crystallogr. E*, 2005, **61**, m1088–m1089.
- 108 L. Wang, M. Yu, L.-Z. Liu, J.-X. Ma and W.-K. Dong, *Z. Kristallogr. NCS*, , DOI:10.1515/ncrs-2017-0390.
- 109 S. Chattopadhyay, M. G. B. Drew and A. Ghosh, *Polyhedron*, 2007, **26**, 3513–3522.
- 110 P. Mukherjee, M. G. B. Drew and A. Ghosh, *Eur. J. Inorg. Chem.*, 2008, **2008**, 3372–3381.
- 111 A. Chakravorty, J. P. Fennessey and R. H. Holm, *Inorg. Chem.*, 1965, **4**, 26–33.
- 112 L. Sacconi, N. Nardi and F. Zanobini, *Inorg. Chem.*, 1966, **5**, 1872–1876.
- 113 C. A. Root, B. A. Rising, M. C. VanDerveer and C. F. Hellmuth, *Inorg. Chem.*, 1972, **11**, 1489–1493.
- 114 A. Trujillo, M. Fuentealba, D. Carrillo, C. Manzur and J.-R. Hamon, *J. Organomet. Chem.*, 2009, **694**, 1435–1440.
- 115 A. Trujillo, S. Sinbandhit, L. Toupet, D. Carrillo, C. Manzur and J.-R. Hamon, *J. Inorg. Organomet. Polym. Mater.*, 2008, **18**, 81–99.
- 116 S. Chattopadhyay, M. S. Ray, S. Chaudhuri, G. Mukhopadhyay, G. Bocelli, A. Cantoni and A. Ghosh, *Inorg. Chim. Acta*, 2006, **359**, 1367–1375.
- 117 P. Bhowmik, M. G. B. Drew and S. Chattopadhyay, *Inorg. Chim. Acta*, 2011, **366**, 62–67.
- 118 A. W. Kleij, *Eur. J. Inorg. Chem.*, 2009, **2009**, 193–205.
- 119 L. Rigamonti, A. Cinti, A. Forni, A. Pasini and O. Piovesana, *Eur. J. Inorg. Chem.*, 2008, **2008**, 3633–3647.
- 120 L. Rigamonti, A. Forni, R. Pievo, J. Reedijk and A. Pasini, *Inorg. Chim. Acta*, 2012, **387**, 373–382.
- 121 L. Rigamonti, A. Forni, M. Sironi, A. Ponti, A. M. Ferretti, C. Baschieri and A. Pasini, *Polyhedron*, 2018, **145**, 22–34.
- 122 N. Matsumoto, S. Yamashita, A. Ohyoshi, S. Kohata and H. Ōkawa, *J. Chem. Soc., Dalton Trans.*, 1988, 1943–1948.
- 123 T. Nozaki, H. Ushio, G. Mago, N. Matsumoto, H. Ōkawa, Y. Yamakawa, T. Anno and T. Nakashima, *J. Chem. Soc., Dalton Trans.*, 1994, 2339–2345.
- 124 T. Nozaki, N. Matsumoto, H. Okawa, H. Miyasaka and G. Mago, *Inorg. Chem.*, 1995, **34**, 2108–2112.
- 125 M. Mimura, T. Matsuo, N. Matsumoto, S. Takamizawa, W. Mori and N. Re, *Bull. Chem. Soc. Jpn.*, 1998, **71**, 1831–1837.
- 126 U. Dinjus, H. Stahl and E. Uhlig, *Z. Anorg. Allg. Chem.*, 1980, **464**, 37–44.
- 127 D.-H. Shi, Z.-L. You, C. Xu, Q. Zhang and H.-L. Zhu, *Inorg. Chem. Commun.*, 2007, **10**, 404–406.
- 128 P. Mukherjee, M. G. B. Drew, V. Tangoulis, M. Estrader, C. Diaz and A. Ghosh, *Polyhedron*, 2009, **28**, 2989–2996.
- 129 L. Rigamonti and A. Forni, *Inorg. Chim. Acta*, 2018, **473**, 216–222.
- 130 D. Cremer and J. A. Pople, *J. Am. Chem. Soc.*, 1975, **97**, 1354–1358.
- 131 M. Nardelli, *J. Appl. Crystallogr.*, 1995, **28**, 659–659.

- 132 L. C. Nathan, J. E. Koehne, J. M. Gilmore, K. A. Hannibal, W. E. Dewhirst and T. D. Mai, *Polyhedron*, 2003, **22**, 887–894. View Article Online
DOI: 10.1039/C9DT01216H
- 133 Ren-Gen Xiong, Bao-Lin Song, Jing-Lin Zuo, Xiao-Zeng You and Xiao-Ying Huang, *Polyhedron*, 1996, **15**, 903–907.
- 134 C. Arici, F. Ercan, R. Kurtaran and O. Atakol, *Acta Crystallogr. C*, 2001, **57**, 812–814.
- 135 G. Consiglio, S. Failla, P. Finocchiaro, I. P. Oliveri, R. Purrello and S. Di Bella, *Inorg. Chem.*, 2010, **49**, 5134–5142.
- 136 G. Consiglio, S. Failla, P. Finocchiaro, I. P. Oliveri and S. D. Bella, *Dalton Trans.*, 2012, **41**, 387–395.
- 137 G. Consiglio, I. P. Oliveri, F. Punzo, A. L. Thompson, S. Di Bella and S. Failla, *Dalton Trans.*, 2015, **44**, 13040–13048.
- 138 Giuseppe Consiglio, Ivan Oliveri, Salvatore Failla and Santo Di Bella, *Inorganics*, 2018, **6**, 8.
- 139 G. Salassa, M. J. J. Coenen, S. J. Wezenberg, B. L. M. Hendriksen, S. Speller, J. A. A. W. Elemans and A. W. Kleij, *J. Am. Chem. Soc.*, 2012, **134**, 7186–7192.
- 140 G. Forte, I. P. Oliveri, G. Consiglio, S. Failla and S. Di Bella, *Dalton Trans.*, 2017, **46**, 4571–4581.
- 141 M. Odoko, N. Tsuchida and N. Okabe, *Acta Crystallogr. E*, 2006, **62**, m708–m709.
- 142 S. Di Bella and I. Fragalà, *New J. Chem.*, 2002, **26**, 285–290.
- 143 B. Kirtman and B. Champagne, *Int. Rev. Phys. Chem.*, 1997, **16**, 389–420.
- 144 S. J. A. van Gisbergen, J. G. Snijders and E. J. Baerends, *J. Chem. Phys.*, 1998, **109**, 10644–10656.
- 145 H. Hait Heinze, F. Della Sala and A. Görling, *J. Chem. Phys.*, 2002, **116**, 9624–9640.
- 146 P. Salek, O. Vahtras, T. Helgaker and H. Ågren, *J. Chem. Phys.*, 2002, **117**, 9630–9645.
- 147 J. L. Oudar and D. S. Chemla, *J. Chem. Phys.*, 1977, **66**, 2664–2668.
- 148 A. Gonciarz, M. Żuber and J. Zwoździak, *ChemistryOpen*, 2018, **7**, 677–687.
- 149 A. Willetts, J. E. Rice, D. M. Burland and D. P. Shelton, *J. Chem. Phys.*, 1992, **97**, 7590–7599.
- 150 M. Fuentealba, J.-R. Hamon, D. Carrillo and C. Manzur, *New J. Chem.*, 2007, **31**, 1815–1825.
- 151 J. Cisterna, V. Dorcet, C. Manzur, I. Ledoux-Rak, J.-R. Hamon and D. Carrillo, *Inorg. Chim. Acta*, 2015, **430**, 82–90.
- 152 J. Cisterna, V. Artigas, M. Fuentealba, P. Hamon, C. Manzur, V. Dorcet, J.-R. Hamon and D. Carrillo, *Inorg. Chim. Acta*, 2017, **462**, 266–280.

Table of Contents Entry

View Article Online
DOI: 10.1039/C9DT01216H

Push-pull unsymmetrical substitution efficiently modulates the electronic, linear and nonlinear optical properties of nickel(II) complexes with salen-type ligands.